Archive of Applied Mechanics
https://doi.org/10.1007/s00419-023-02497-y

ORIGINAL

Nathan Perchikov · **Jacob Aboudi** · **Konstantin Y. Volokh**

Finite strain HFGMC analysis of damage evolution in nonlinear periodic composite materials

Received: 22 March 2023 / Accepted: 20 September 2023

Abstract This work studies the evolution of damage in periodic composites with hyperelastic constituents prone to mechanical degradation under sufficient loading. The micromechanical problem is solved for quasistatic far-field loading for plane-strain conditions, using the finite strain high-fidelity general method of cells (FSHFGMC) approach to discretize the conservation equations. Damage is treated as degradation of material cohesion, modeled by a material conservation law with a stress-dependent damage-source (sink) term. The two-way coupled formulation with the internal variable representing damage is reminiscent of the phase-field approach to gradual cracks growth, albeit with a mechanistically derived governing equation, and with important theoretical differences in consequences. The HFGMC approach consists in enforcing equilibrium in each phase (in the cell-average sense) by stress linearization, using instantaneous tangent moduli, and subsequent iterative enforcement of continuity conditions, a formulation arguably natural for composite materials. The inherent stiffness of the underlying differential equations is treated by use of a predictor–corrector scheme. Various examples are solved, including those of porous material developing cracks close to the cavity, for various sizes and shapes of the cavity, damage in a two-phase composite of both periodic and random structure, etc. The proposed methodology is physically tractable and numerically robust and allows various generalizations.

Keywords Micromechanics · Composite · Hyperelastic · Phase-field · Damage · HFGMC

1 Introduction

In the present investigation, the finite strain high-fidelity generalized method of cells (FSHFGMC) is employed for micromechanical analysis of evolution of damage in composites, the phases of which are hyperelastic in the undamaged state. The micromechanical analysis is designated to establish the global behavior of composite materials undergoing large deformations, and also the field distributions among the composite's constituents. It is applicable for composites possessing periodic microstructure such that a repeating unit cell (RUC) can be identified.

In what concerns analysis of material degradation in composites employing the increasingly popular phase-field approach, several works should be noted. In Borden et al. [8], an extensive numerical study was performed,

N. Perchikov (✉) · J. Aboudi
School of Mechanical Engineering, Faculty of Engineering, Tel Aviv University, 69978 Tel Aviv, Israel
E-mail: perchico@gmail.com

J. Aboudi
E-mail: aboudi@eng.tau.ac.il

K. Y. Volokh
Faculty of Civil Engineering, Technion – Israel Institute of Technology, 32000 Haifa, Israel
E-mail: cvolokh@technion.ac.il

Published online: 10 October 2023

using a phase-field equation regularizing sharp cracks, starting from one-dimensional analysis and proceeding to 2D and 3D, using staggered and monolithic time-stepping schemes for the dynamic fracture scenario, employing adaptive mesh refinement and obtaining characteristic crack-branching approximating patterns.

In Zhang et al. [29], finite-element analysis of a composite undergoing gradual failure was performed. There, to compensate for the automatic continuity of stresses between the constituents, inherent to the FE formulation, a phase-field was introduced in the interface between the matrix and inclusions. In addition, cracks were accounted for by their own phase fields, whose energy was included in the formulation in a standard square gradient form. A noteworthy study is presented in Guillén–Hernández et al. [16], where composites with randomly positioned identical long fibers in a matrix undergo gradual damage in the form of cracks modeled by a phase-field obeying the standard source-less screened Poisson equation with a constant screening parameter, albeit with effective damaged area represented by the square of the phase-field. Characteristic effective stress decrease and non-sharp damage zone are obtained. In Dean et al. [12], finite-element analysis is performed for long-fiber laminate-composites, with two phase fields, one for describing delamination at the interface between fibers and the matrix, and one for plastic fracture in the matrix. The fracture-approximating phase-field is represented in the energy in the standard squared-gradient form. Several examples are shown, with characteristic homogenized stress response curves, concave up to a maximum, and convexly decreasing afterward due to damage. In Denli et al. [13], nonlinear isotropic finite-element analysis was performed, also with squared phase-field damaged area, albeit with an evolution equation for the phase-field, with a slow limit in the form of a screened Poisson equation with an energy-dependent screening coefficient. In Tarafder et al. [25], finite-element analysis of matrix-inclusion composites with random microstructure was conducted using a standard constant-coefficient linear second-order equation for the phase-field representing the cohesion zone, showing the emergence of crack-like damage zones and global stress–strain response with a decreasing part and additional strain hardening for further loading. A recent comprehensive review of application of various phase-field models for the description of damage evolution in fiber-reinforced laminated composites is given in Bui and Hu [11]. A formulation similar to Tarafder et al. [25] recently showed very sharp crack-like damage patterns in Sangaletti and Garciá [24]. An insightful recent one-dimensional analysis of microstructure evolution in composites applying phase-field modeling with stiffness degradation, presenting non-trivial crack-like patterns and global stress–strain response, is given in Rao et al. [23]. In Quinteros et al. [22], crack initiation in composites reinforced by carbon nano-tubes (CNT) is investigated using a phase-field model with quadratic damaged area phase-field dependence and a Poisson equation with a constant screening coefficient. The equilibrium and phase-field equations are solved in finite-element discretization, using the BFGS quasi-Newton optimization algorithm. Noteworthy crack patterns and effective stress-displacement curves are obtained.

The FSHFGMC has been employed by Aboudi [1] to establish the behavior of rubber-like composites which exhibit the Mullins effect in Mullins and Tobin [20]. It was also implemented to predict the behavior of biological tissues in Breiman et al. [9]. In order to model the evolution of damage in composite materials undergoing finite strains, the concept of an energy limiter (see Volokh [26], for example) has been incorporated into the FSHFGMC micromechanical analysis. The resulting studies of elastic, Aboudi and Volokh [3], and viscoelastic, Aboudi and Volokh [4], composites, in which the FSHFGMC was employed with embedded energy limiters, show that the failure of composite can be reasonably well predicted by this approach. In a more recent investigation, Breiman et al. [10], the non-orthogonal version of FSHFGMC, in conjunction with the energy limiter, has been applied for the prediction of damage evolution and failure of composites with wavy interfaces between the constituents.

In the framework of the HFGMC, the RUC is divided into an arbitrary number of subcells each of which contains distinct homogeneous material. In every subcell, the displacement increments are expanded into second-order Legendre polynomials of the coordinates with the coefficients being the microvariables. The governing equations are implemented for each subcell in the volume-average sense. The continuity of the increments in displacements and tractions at the surfaces between neighboring subcells is imposed in the surface-average sense. A similar approach is taken with the periodicity conditions on the displacements and tractions increments at the opposite edges of the RUC. As a result, a system of algebraic equations for the unknown microvariables is obtained, the solution of which is then employed to obtain the global response of the composite, as well as the fields within each subcell. Detailed discussions, verifications and applications of the FSHFGMC to elastic, viscoelastic, viscoplastic and thermoviscoelastic composites can be found in chapter 9 of Aboudi et al. [2].

In the present article, the FSHFGMC methodology is generalized, and the displacements and intact material fraction increments in each subcell are both expanded into second-order Legendre polynomials of the

coordinates. Balance equations are imposed in every subcell of the RUC in a volumetric sense. The continuity and periodicity conditions for the increments in the displacements, tractions and the damage variable and its fluxes are imposed in the surface-average sense. This system of coupled equations is solved by implementing a predictor–corrector procedure which provides the unknown microvariable increments at every step of the far-field loading. The various fields are then established from the computed microvariable increments.

The proposed predictor–corrector scheme has some resemblance to the one given in Hofacker and Miehe [17], where it is implemented with a staggered multi-field finite-element approach, albeit for linear elastic homogeneous materials in the rate-dependent loading case. Here, instead, a composite material of periodic microstructure is addressed and inertia is neglected (quasistatic loading).

An important feature of the FSHFGMC, when compared to finite-element methods, is that here the governing (conservation) equations are imposed explicitly (analytically) in incremental form, although in the cell-averaged sense, and the resulting system to be solved numerically is that of continuity of fields between the constituents of the composite. In contrast, in finite-element methods, the approximation is constructed such that continuity would hold automatically, and the conservation equations are solved iteratively (even if by sequential Gauss elimination). This difference between the approaches is rooted in the physical understanding of the difference between mechanical composites and homogeneous structural materials. It can be argued that the stress homogeneity is reached in a continuum faster than mechanical equilibrium. First, the notion of stress becomes meaningful, and only then its divergence complies with the equilibrium equation. Therefore, it is natural, when analyzing homogeneous materials, to assume continuous fields, which are iteratively driven to equilibrium. Moreover, in a homogeneous material, there are no natural discontinuities. In contrast, in a composite, it is evident that the contact between constituents is not perfect, especially without sufficient compressive stress. Therefore, it is natural to assume each homogeneous constituent being in immediate mechanical equilibrium, on average, when 'probing' on the scale of a subcell, and then, gradually, additional fluctuations emerge on the subcell level, which enforce subcell-level continuity and eventually continuity along the interfaces between the different constituents. The reason to assume that in-phase equilibrization is faster than inter-phase continuity attainment is that the in-phase bonds are stronger than inter-phase bonds, and stronger bonds are normally associated with faster relaxation times, hence the assumption that equilibrium in the phase is attained before continuity between the phases.

The present work opts to employ an approach in which both coupling directions emerge from a statistical mechanistic understanding, resorting to the recently suggested Material Sink Model applied for simulation of crack initiation in Volokh [27], Faye et al. [15] and Abu-Qbeitah et al. [5,6]. In this approach, the damaged area is represented as a phase-field-like variable, and the equation for this variable is similar to the screened Poisson equation, albeit with a non-constant screening parameter, which unlike in the mentioned works, *strongly* depends on the local energy density.

The following section outlines the governing equations. Section 3 presents the finite strain micromechanical theory (discretization of the problem). Section 4 describes the method of solution of the discretized problem. Applications of the method are given in Sect. 5. Discussion of the results is conducted in Sect. 6. Section 7 concludes.

2 Governing equations

Let the elastic strain energy density in intact solid material be denoted by W and the deformation gradient be given by $\mathbf{F}$. The effective transposed first Piola–Kirchhoff stress tensor $\mathbf{P}$ is given by (see Menikoff and Kober [19], for example):

$$\mathbf{P} = \theta \frac{\partial W}{\partial \mathbf{F}} \tag{1}$$

where $\theta = \frac{\rho_i}{\rho_0} = \frac{m_i/V_0}{m_0/V_0} = \frac{\rho_0 V_i}{\rho_0 V_0}$ is the mass (in a control volume) or volume (in a given mass) fraction of material in *intact* (undamaged) state (assuming that the density of intact material, ρ_0, is nearly constant throughout the deformation process). Here, V_i refers to the volume of a box containing a statistically representative chunk of partially damaged matter, V_0 refers to the volume of the intact matter inside the said box, ρ_i refers to the mass of intact matter divided by the volume of the said box, and ρ_0 refers to the mass of the intact matter divided by the volume of intact matter, V_0, inside the said box.

The proportionality of the stress to θ reflects the assumption that all stress is carried by intact material, and damage is associated with full loss of ability to hold stress. The factor θ is both the average volume of intact material and the areal fraction of intact material in an *average* cross section.

The first Piola–Kirchhoff stress tensor $\mathbf{T}$, Malvern [18], is then given by the transpose of $\mathbf{P}$:

$$\mathbf{T} = \mathbf{P}^T \tag{2}$$

The increment in $\mathbf{P}$ is:

$$\Delta\mathbf{P} = \theta\mathbf{R}\Delta\mathbf{F} + \mathbf{H}\Delta\theta \tag{3}$$

where the tangent tensor $\mathbf{R}$ and tensor $\mathbf{H}$ are given by

$$\mathbf{R} = \frac{\partial^2 W}{\partial \mathbf{F}^2}, \quad \mathbf{H} = \frac{\partial W}{\partial \mathbf{F}} \tag{4}$$

Thus,

$$\Delta W = H_{ij}\Delta F_{ij}, \quad i, j = 1, 2, 3 \tag{5}$$

Let the following two vectors be defined as follows:

$$\begin{aligned} \Delta\boldsymbol{\Omega} &= [\Delta F_{11}, \Delta F_{12}, \Delta F_{13}, \Delta F_{21}, \Delta F_{22}, \Delta F_{23}, \Delta F_{31}, \Delta F_{32}, \Delta F_{33}] \\ \Delta\boldsymbol{\Sigma} &= [\Delta T_{11}, \Delta T_{12}, \Delta T_{13}, \Delta T_{21}, \Delta T_{22}, \Delta T_{23}, \Delta T_{31}, \Delta T_{32}, \Delta T_{33}] \end{aligned} \tag{6}$$

Then, constitutive equation (3) can be written in the matrix form:

$$\Delta\boldsymbol{\Sigma} = \mathbf{Z}\,\Delta\boldsymbol{\Omega} + \mathbf{H}\Delta\theta \tag{7}$$

where $\mathbf{Z}$ is the ninth-order instantaneous matrix of the material which can be constructed from the tangent tensor $\mathbf{R}$ and θ.

The normalized mass flux $\mathbf{S}$ of damaged material (crumbs) is given by

$$\mathbf{S} = -\bar{l}^2\nabla(1-\theta) = \bar{l}^2\nabla\theta \tag{8}$$

where $\bar{l}$ is an appropriate coefficient, representing the characteristic length scale of damage concentration[1]. This relation can be written in an incremental form as:

$$\Delta\mathbf{S} = \bar{l}^2\nabla\Delta\theta \tag{9}$$

The incremental equilibrium equations are:

$$\Delta T_{ij,i} = 0, \quad i, j = 1, 2, 3 \tag{10}$$

The (normalized) mass balance equation for the crumbled (damaged) material (where the divergence term represents the contribution of the essentially entropic force causing the spread of the crumbs) reads:

$$\theta\zeta - \nabla\cdot\mathbf{S} = const. = 1 \tag{11}$$

where $\theta\zeta$ is a source term representing the rate of production of damaged material (crumbs) by intact material (hence the proportionality to θ, in accordance with the proportionality of stress to θ), and where the rate factor ζ increases super-exponentially with the energy density in the intact material, namely

$$\zeta = \exp\left[\left(\frac{W}{\phi}\right)^m\right] \tag{12}$$

[1] The physical interpretation of the mass flux term can be that crumbs will push each other from the locus of their generation, since there would be no significant attraction forces between them, only repelling forces. Therefore, phenomenologically, eventually there would be a flow of them in the direction opposite to the gradient, the same way it happens with heat (it can be argued that the crumbs will spread due to the entropic principle, or the Liouville dynamical principle, and the spreading would be away from the generation points, or in the direction opposite to the gradient).

Here, $\phi > 0$ is a material parameter, related to material bond energy, and $m > 1$ is a numerical constant, related the level of spatial localization of damage.

The constant on the right-hand side of the balance law (11) can be interpreted to represent an average (over a time scale much smaller than the characteristic time scale of continuum deformation) of the rate of change of the relative amount of damaged material (crumbs) in a control volume. The balance law (11) provides an equation for θ on the large time scale of continuum deformation, for which the specific distribution of fast individual bond ruptures is not important. The average of the fast dynamics over the rate term that would have been on the right-hand side, namely $\dot{\theta}$, amounts to a constant on the large time scale[2]. The value of the constant is then normalized to be 1 with the interpretation of ζ^{-1} as the homogeneous case expression for θ, namely θ_h. The super-exponentially decaying dependence on energy for θ_h is reasoned as follows. Equilibrium processes normally show exponentially decaying dependence on energy, and are exhibiting spatial uniformity. An inequilibrium process, such as damage, should arguably have a stronger spatial localization, as observed empirically, and a super-exponential function is a natural form to represent this. As for the left-hand side of the balance law (11), it is linear in θ, and moreover, W and thus ζ are constant on the fast time scale of rupture, and hence averaging on a fast time scale does not alter the equation (when θ is then renamed to represent already its own fast time average).

As aforementioned, the equation is written such that ζ^{-1} would represent the *expected value* of θ_h (based on its probability distribution not specified in the employed continuum-level model). This quantity is constructed to give unity for $W = 0$, if there is no preexisting (damage).

To avoid numerical overflow, in practice, $(\zeta^{-1} + \epsilon)^{-1}$ is used in this work instead of ζ, with the choice $\epsilon = 10^{-20}$.

The incremental form of (-1 times) the balance equation then reads:

$$\frac{\partial \Delta S_1}{\partial X_1} + \frac{\partial \Delta S_2}{\partial X_2} + \frac{\partial \Delta S_3}{\partial X_3} - \frac{\Delta\theta}{\zeta^{-1} + \epsilon} - \frac{\theta}{(1 + \epsilon\zeta)^2}\Delta\zeta = 0 \tag{13}$$

with

$$\Delta\zeta = \frac{m}{\phi}\left(\frac{W}{\phi}\right)^{m-1} \zeta\ \Delta W \tag{14}$$

The interfacial conditions are:

$$[[\Delta \mathbf{T}^T]] \cdot \mathbf{N} = \mathbf{0}, \quad [[\Delta \mathbf{u}]] = \mathbf{0} \tag{15}$$

and

$$[[\Delta \mathbf{S}]] = \mathbf{0}, \quad [[\Delta\theta]] = 0 \tag{16}$$

It should be mentioned here that the described damage model can in principle be appropriate for various materials, where specific features can yield additional components to the description. For example, for brittle crystalline materials, an additional feature in the model can be stress asymmetry in the source term, such that only positive stretch would result in damage. For the case of polymeric materials, due to the complicated nonlinear microstructure, it is expected that even isotropic compression on the continuum scale could be translated into shear and positive stretch for individual chains, resulting in damage for critical pressure values. Therefore, it may be adequate not to draw a distinction based on stress orientation but condition the damage solely on the accumulated strain energy. This approach was followed for the aortic abdominal aneurysm material (see Faye et al. [15]), which is employed in the examples solved in the present work.

Another noteworthy point concerns the way to determine the damage model parameters. The topic is discussed in Volokh [27] and in Faye et al. [15]. In principle, the parameters $\bar{l}$ and m describe the level of localization of damage and ϕ describes the bond energy density. In the present study, the value of ϕ was taken to be the same as in Abu-Qbeitah et al. [5]. The value of ϕ should be related to the values of C_1, C_2 in a manner that should be determined in comparison with experiments, as discussed in Faye et al. [15]. The

[2] The left-hand side includes the smooth part of crumbs transport, which makes no contribution in a short period, and the nonsmooth source term, which makes contribution proportional to the number of rupture events in the short period. The probability for a certain number of rupture events in a continuum-level timescale Δt can be assumed to have Gaussian distribution, rather than, say, a power-law-tailed distribution, since the problem is not scale-free, like, say, plasticity, a fact indicated by the divergence operator and $\bar{l}$. Consequently, the amount of rupture in Δt is integrable (an integral over Δt of a fixed/typical number of delta functions yields a constant).

localization parameters were chosen here from general considerations. In order to present inequilibrium-level localization, one has to choose $m > 1$. The value $m = 2$ is already feasible; however, to check convergence, a yet higher value should be checked. Noninteger values are also possible, but the dependence on m is not strong enough to justify it. The value of $\bar{l}$ should be significantly smaller than the computational element size (subcell length here). The typical element size in mechanical calculations is millimetric, hence the choice of $\bar{l}$ to be submillimetric is feasible. However, as shown in Volokh [27], for some materials, the proper determination of material parameters consists in choosing an adequate, high-enough value of m, and then establishing $\bar{l}$ and ϕ by fitting to experimental data, such as a uniaxial stress tension test up to global rupture of a specimen of proper size, for which the constants C_1, C_2 have been predetermined. As mentioned in Volokh [27], the value of $\bar{l}$ can vary from 0.2mm for rubber to 2.6cm for concrete. When comparing a calculation based on the model with a test, $\bar{l}$ should fit the rupture thickness as observed, ϕ then to the rupture force (implicitly). As for m, it should determine temporal localization, i.e., time from onset to end of rupture in a quasistatic experiment (or a dynamic one, using the dynamic analysis as discussed in Abu-Qbeitah et al. [5]). Of course, m bears effect also on the level of spatial localization of the rupture zone, hence an appropriate value of $\bar{l}$ is expected for every adequate choice of m.

3 Finite strain micromechanical analysis

Consider a multiphase composite in which the phases are undergoing large deformations. It is assumed that the composite microstructures are distributed in a doubly periodic manner and are described with respect to the global initial coordinates (X_1, X_2, X_3), see Fig. 1a. Figure 1b shows a repeating unit cell (RUC), defined with respect to local initial coordinates (Y_2, Y_3), of the periodic composite. Herein, the finite strain HFGMC micromechanical model is employed to predict the behavior of the composite caused by the application of external mechanical loading. The rectangular RUC of the composite is divided into N_β and N_γ subcells in the Y_2 and Y_3 directions, respectively. Each subcell is labeled by the indices $(\beta\gamma)$ with $\beta = 1, ..., N_\beta$ and $\gamma = 1, ..., N_\gamma$. The dimensions of subcell $(\beta\gamma)$ in the Y_2 and Y_3 directions are denoted by h_β and l_γ, respectively. A local coordinate system $(\bar{Y}_2^{(\beta)}, \bar{Y}_3^{(\gamma)})$ is introduced in each subcell whose origin is located at its center, see Fig. 1c.

In the framework of HFGMC analysis which is presently employed to predict the behavior of the considered composites, the increments in the mechanical displacements $\Delta\mathbf{u}^{(\beta\gamma)}$ in the subcell $(\beta\gamma)$ are expanded into second-order polynomials. To this end, let the vector $\Delta\mathbf{W}^{(\beta\gamma)}$ represent the components of the displacement vector $\Delta\mathbf{u}^{(\beta\gamma)}$:

$$\Delta\mathbf{W}^{(\beta\gamma)} = [\Delta u_1, \Delta u_2, \Delta u_3]^{(\beta\gamma)} \tag{17}$$

The second-order expansion is given by

$$\begin{aligned}\Delta\mathbf{W}^{(\beta\gamma)} = {} & \Delta\bar{\mathbf{W}} + \Delta\mathbf{W}_{(00)}^{(\beta\gamma)} + \bar{Y}_2^{(\beta)}\Delta\mathbf{W}_{(10)}^{(\beta\gamma)} + \bar{Y}_3^{(\gamma)}\Delta\mathbf{W}_{(01)}^{(\beta\gamma)} \\ & + \frac{1}{2}\left(3\bar{Y}_2^{(\beta)2} - \frac{h_\beta^2}{4}\right)\Delta\mathbf{W}_{(20)}^{(\beta\gamma)} + \frac{1}{2}\left(3\bar{Y}_3^{(\gamma)2} - \frac{l_\gamma^2}{4}\right)\Delta\mathbf{W}_{(02)}^{(\beta\gamma)}\end{aligned} \tag{18}$$

where $\Delta\bar{\mathbf{W}} = [\Delta\bar{\mathbf{F}} \cdot \mathbf{X}]$ consists of the externally applied loading.

Similarly,

$$\begin{aligned}\Delta\theta^{(\beta\gamma)} = {} & \Delta\theta_{(00)}^{(\beta\gamma)} + \bar{Y}_2^{(\beta)}\Delta\theta_{(10)}^{(\beta\gamma)} + \bar{Y}_3^{(\gamma)}\Delta\theta_{(01)}^{(\beta\gamma)} \\ & + \frac{1}{2}\left(3\bar{Y}_2^{(\beta)2} - \frac{h_\beta^2}{4}\right)\Delta\theta_{(20)}^{(\beta\gamma)} + \frac{1}{2}\left(3\bar{Y}_3^{(\gamma)2} - \frac{l_\gamma^2}{4}\right)\Delta\theta_{(02)}^{(\beta\gamma)}\end{aligned} \tag{19}$$

The unknown coefficients $\Delta\mathbf{W}_{(mn)}^{(\beta\gamma)}$ and $\Delta\theta_{(mn)}^{(\beta\gamma)}$ are determined, as shown in the following, by implementing the equilibrium equations (10) and the mass balance (13) together with the interfacial continuity conditions (15)–(16), and periodic conditions, which are discussed below.

In the framework of the HFGMC micromechanical analysis, periodic boundary conditions must be imposed to ensure the periodic microstructure character of the composite as represented by the repeating unit cell of

Fig. 1b. These conditions require that the increments in the displacement vectors $\mathbf{u}$ and the traction vectors $\mathbf{T}^{\mathbf{N}} = \mathbf{T}^T \cdot \mathbf{N}$ at the opposite edges of the repeating unit cell are identical. This implies that:

$$\begin{aligned} \Delta\mathbf{u}(Y_2 = 0) &= \Delta\mathbf{u}(Y_2 = 2h), \quad & \Delta\mathbf{T}^{\mathbf{N}}(Y_2 = 0) &= \Delta\mathbf{T}^{\mathbf{N}}(Y_2 = 2h) \\ \Delta\mathbf{u}(Y_3 = 0) &= \Delta\mathbf{u}(Y_3 = 2l), \quad & \Delta\mathbf{T}^{\mathbf{N}}(Y_3 = 0) &= \Delta\mathbf{T}^{\mathbf{N}}(Y_3 = 2l) \end{aligned} \tag{20}$$

Similarly,

$$\begin{aligned} \Delta\theta(Y_2 = 0) &= \Delta\theta(Y_2 = 2h), \quad & \Delta S_2(Y_2 = 0) &= \Delta S_2(Y_2 = 2h) \\ \Delta\theta(Y_3 = 0) &= \Delta\theta(Y_3 = 2l), \quad & \Delta S_3(Y_3 = 0) &= \Delta S_3(Y_3 = 2l) \end{aligned} \tag{21}$$

The components of the increments in the deformation gradient tensor $\Delta\mathbf{F}^{(\beta\gamma)}$ in the subcell $(\beta\gamma)$ are determined from Eq. (18) by applying the relevant derivatives with respect to the local coordinates, as follows.

$$\begin{aligned} \Delta F_{11}^{(\beta\gamma)} &= \Delta\bar{F}_{11} \\ \Delta F_{12}^{(\beta\gamma)} &= \Delta\bar{F}_{12} + \Delta W_{1(10)}^{(\beta\gamma)} + 3\bar{Y}_2^{(\gamma)}\Delta W_{1(20)}^{(\beta\gamma)} \\ \Delta F_{13}^{(\beta\gamma)} &= \Delta\bar{F}_{13} + \Delta W_{1(01)}^{(\beta\gamma)} + 3\bar{Y}_3^{(\gamma)}\Delta W_{1(02)}^{(\beta\gamma)} \\ \Delta F_{21}^{(\beta\gamma)} &= \Delta\bar{F}_{21} \\ \Delta F_{22}^{(\beta\gamma)} &= \Delta\bar{F}_{22} + \Delta W_{2(10)}^{(\beta\gamma)} + 3\bar{Y}_2^{(\gamma)}\Delta W_{2(20)}^{(\beta\gamma)} \\ \Delta F_{23}^{(\beta\gamma)} &= \Delta\bar{F}_{23} + \Delta W_{2(01)}^{(\beta\gamma)} + 3\bar{Y}_3^{(\gamma)}\Delta W_{2(02)}^{(\beta\gamma)} \\ \Delta F_{31}^{(\beta\gamma)} &= \Delta\bar{F}_{31} \\ \Delta F_{32}^{(\beta\gamma)} &= \Delta\bar{F}_{32} + \Delta W_{3(10)}^{(\beta\gamma)} + 3\bar{Y}_2^{(\gamma)}\Delta W_{3(20)}^{(\beta\gamma)} \\ \Delta F_{33}^{(\beta\gamma)} &= \Delta\bar{F}_{33} + \Delta W_{3(01)}^{(\beta\gamma)} + 3\bar{Y}_3^{(\gamma)}\Delta W_{3(02)}^{(\beta\gamma)} \end{aligned} \tag{22}$$

The components of the gradient of $\Delta\theta^{(\beta\gamma)}$ in the subcell $(\beta\gamma)$ are determined from Eq. (19) by applying the relevant derivatives with respect to the local coordinates, as follows.

$$\begin{aligned} \Delta\theta_{,2}^{(\beta\gamma)} &= \Delta\theta_{2(10)}^{(\beta\gamma)} + 3\bar{Y}_2^{(\beta)}\Delta\theta_{2(20)}^{(\beta\gamma)} \\ \Delta\theta_{,3}^{(\beta\gamma)} &= \Delta\theta_{3(01)}^{(\beta\gamma)} + 3\bar{Y}_3^{(\gamma)}\Delta\theta_{3(02)}^{(\beta\gamma)} \end{aligned} \tag{23}$$

By averaging the increments in the equilibrium equations (10) over the area of the subcell, the following relations are obtained:

$$\Delta\mathbf{I}_{2(00)}^{(\beta\gamma)} + \Delta\mathbf{I}_{3(00)}^{(\beta\gamma)} = 0 \tag{24}$$

where $\Delta\mathbf{I}_{2(00)}^{(\beta\gamma)}$ and $\Delta\mathbf{I}_{3(00)}^{(\beta\gamma)}$ can be expressed in terms of the surface averages of the traction increments evaluated along $\bar{Y}_2^{(\beta)} = \pm h_\beta/2$ and $\bar{Y}_3^{(\gamma)} = \pm l_\gamma/2$, respectively. Thus,

$$\begin{aligned} \Delta\mathbf{I}_{2(00)}^{(\beta\gamma)} &= \frac{1}{h_\beta}\left[\Delta\mathbf{T}_2^{+(\beta\gamma)} - \Delta\mathbf{T}_2^{-(\beta\gamma)}\right] \\ \Delta\mathbf{I}_{3(00)}^{(\beta\gamma)} &= \frac{1}{l_\gamma}\left[\Delta\mathbf{T}_3^{+(\beta\gamma)} - \Delta\mathbf{T}_3^{-(\beta\gamma)}\right] \end{aligned} \tag{25}$$

where the surface averages of the tractions increments are given by

$$\begin{aligned} \Delta\mathbf{T}_2^{\pm(\beta\gamma)} &= \frac{1}{l_\gamma}\int_{-l_\gamma/2}^{l_\gamma/2} \Delta\boldsymbol{\Sigma}_2^{(\beta\gamma)}\left(\bar{Y}_2^{(\beta)} = \pm\frac{h_\beta}{2}\right) d\bar{Y}_3^{(\gamma)} \\ \Delta\mathbf{T}_3^{\pm(\beta\gamma)} &= \frac{1}{h_\beta}\int_{-h_\beta/2}^{h_\beta/2} \Delta\boldsymbol{\Sigma}_3^{(\beta\gamma)}\left(\bar{Y}_3^{(\gamma)} = \pm\frac{l_\gamma}{2}\right) d\bar{Y}_2^{(\beta)} \end{aligned} \tag{26}$$

and

$$\Delta\boldsymbol{\Sigma}_2^{(\beta\gamma)} = [\Delta T_{21}, \Delta T_{22}, \Delta T_{23}]^{(\beta\gamma)}$$
$$\Delta\boldsymbol{\Sigma}_3^{(\beta\gamma)} = [\Delta T_{31}, \Delta T_{32}, \Delta T_{33}]^{(\beta\gamma)} \tag{27}$$

The two vectors $\Delta\boldsymbol{\Sigma}_2^{(\beta\gamma)}$ and $\Delta\boldsymbol{\Sigma}_3^{(\beta\gamma)}$ include the tractions increments acting on the surfaces whose normals are in the $\bar{Y}_2^{(\beta)}$ and $\bar{Y}_3^{(\gamma)}$ directions, respectively.

Substitution of Eq. (25) in Eq. (24) yields

$$\frac{1}{h_\beta}\left[\Delta\mathbf{T}_2^{+(\beta\gamma)} - \Delta\mathbf{T}_2^{-(\beta\gamma)}\right] + \frac{1}{l_\gamma}\left[\Delta\mathbf{T}_3^{+(\beta\gamma)} - \Delta\mathbf{T}_3^{-(\beta\gamma)}\right] = 0. \tag{28}$$

This equation expresses the increments in the equilibrium equations, imposed in the average sense within subcell $(\beta\gamma)$.

By employing the constitutive relations (7), the following expressions for the surface averages of the traction increments are obtained from Eqs. (22) and (26):

$$\begin{aligned}\Delta T_{2i}^{\pm(\beta\gamma)} = {} & Z_{k2}^{(\beta\gamma)}\left(\Delta W_{1(10)} \pm \frac{3h_\beta}{2}\Delta W_{1(20)}\right)^{(\beta\gamma)} + Z_{k3}^{(\beta\gamma)}\Delta W_{1(01)}^{(\beta\gamma)} \\ & + Z_{k5}^{(\beta\gamma)}\left(\Delta W_{2(10)} \pm \frac{3h_\beta}{2}\Delta W_{2(20)}\right)^{(\beta\gamma)} + Z_{k6}^{(\beta\gamma)}\Delta W_{2(01)}^{(\beta\gamma)} \\ & + Z_{k8}^{(\beta\gamma)}\left(\Delta W_{3(10)} \pm \frac{3h_\beta}{2}\Delta W_{3(20)}\right)^{(\beta\gamma)} + Z_{k9}^{(\beta\gamma)}\Delta W_{3(01)}^{(\beta\gamma)} \\ & + \sum_{p=1}^{9} Z_{kp}^{(\beta\gamma)}\Delta\bar{\Omega}_p + H_{i2}^{(\beta\gamma)}\left(\Delta\theta_{(00)} \pm \frac{h_\beta}{2}\Delta\theta_{(10)} + \frac{3h_\beta}{2}\Delta\theta_{(20)}\right)^{(\beta\gamma)}\end{aligned} \tag{29}$$

where $i = 1 \to k = 4$, $i = 2 \to k = 5$, $i = 3 \to k = 6$.

$$\begin{aligned}\Delta T_{3i}^{\pm(\beta\gamma)} = {} & Z_{k2}^{(\beta\gamma)}\Delta W_{1(10)}^{(\beta\gamma)} + Z_{k3}^{(\beta\gamma)}\left(\Delta W_{1(01)} \pm \frac{3l_\gamma}{2}\Delta W_{1(02)}\right)^{(\beta\gamma)} \\ & + Z_{k5}^{(\beta\gamma)}\Delta W_{2(10)}^{(\beta\gamma)} + Z_{k6}^{(\beta\gamma)}\left(\Delta W_{2(01)} \pm \frac{3l_\gamma}{2}\Delta W_{2(02)}\right)^{(\beta\gamma)} \\ & + Z_{k8}^{(\beta\gamma)}\Delta W_{3(10)}^{(\beta\gamma)} + Z_{k9}^{(\beta\gamma)}\left(\Delta W_{3(01)} \pm \frac{3l_\gamma}{2}\Delta W_{3(02)}\right)^{(\beta\gamma)} \\ & + \sum_{p=1}^{9} Z_{kp}^{(\beta\gamma)}\Delta\bar{\Omega}_p + H_{i3}^{(\beta\gamma)}\left(\Delta\theta_{(00)} \pm \frac{l_\gamma}{2}\Delta\theta_{(01)} + \frac{3l_\gamma}{2}\Delta\theta_{(02)}\right)^{(\beta\gamma)}\end{aligned} \tag{30}$$

where $i = 1 \to k = 7$, $i = 2 \to k = 8$, $i = 3 \to k = 9$. In these equations, $\Delta\bar{\boldsymbol{\Omega}}$ represents the applied far-field:

$$\Delta\bar{\boldsymbol{\Omega}} = \left[\Delta\bar{F}_{11}, \Delta\bar{F}_{12}, \Delta\bar{F}_{13}, \Delta\bar{F}_{21}, \Delta\bar{F}_{22}, \Delta\bar{F}_{23}, \Delta\bar{F}_{31}, \Delta\bar{F}_{32}, \Delta\bar{F}_{33}\right] \tag{31}$$

Substitution of Eqs. (29)–(30) in Eq. (28) provides the three relations:

$$\begin{aligned}&\Big[Z_{22}\Delta W_{1(20)} + Z_{25}\Delta W_{2(20)} + Z_{28}\Delta W_{3(20)} + Z_{33}\Delta W_{1(02)} + Z_{36}\Delta W_{2(02)} + Z_{39}\Delta W_{3(02)} \\ &+ H_{12}\Delta\theta_{(10)} + H_{13}\Delta\theta_{(01)}\Big]^{(\beta\gamma)} = 0\end{aligned} \tag{32}$$

$$\Big[Z_{52}\Delta W_{1(20)} + Z_{55}\Delta W_{2(20)} + Z_{58}\Delta W_{3(20)} + Z_{63}\Delta W_{1(02)} + Z_{66}\Delta W_{2(02)} + Z_{69}\Delta W_{3(02)} + H_{22}\Delta\theta_{(10)} + H_{23}\Delta\theta_{(01)}\Big]^{(\beta\gamma)} = 0 \tag{33}$$

$$\Big[Z_{82}\Delta W_{1(20)} + Z_{85}\Delta W_{2(20)} + Z_{88}\Delta W_{3(20)} + Z_{93}\Delta W_{1(02)} + Z_{96}\Delta W_{2(02)} + Z_{99}\Delta W_{3(02)} + H_{32}\Delta\theta_{(10)} + H_{33}\Delta\theta_{(01)}\Big]^{(\beta\gamma)} = 0 \tag{34}$$

These three relations express the increments in the average equilibrium equations (10) in the subcell, which are given in terms of the increments in the unknown micromechanical variables $\Delta\mathbf{W}^{(\beta\gamma)}_{(mn)}$.

As for the mass flux $\mathbf{S}$, let us define the surface averages of the increments $\Delta\mathbf{S}^{\pm(\beta\gamma)}$ in the subcells as follows:

$$\begin{aligned}\Delta S_2^{\pm(\beta\gamma)} &= \frac{1}{l_\gamma}\int_{-l_\gamma/2}^{l_\gamma/2} \Delta S_2^{(\beta\gamma)}\left(\bar{Y}_2^{(\beta)} = \pm\frac{h_\beta}{2}\right) d\bar{Y}_3^{(\gamma)} \\ \Delta S_3^{\pm(\beta\gamma)} &= \frac{1}{h_\beta}\int_{-h_\beta/2}^{h_\beta/2} \Delta S_3^{(\beta\gamma)}\left(\bar{Y}_3^{(\gamma)} = \pm\frac{l_\gamma}{2}\right) d\bar{Y}_2^{(\beta)}\end{aligned} \tag{35}$$

and

$$\begin{aligned}\Delta J_{2(00)}^{(\beta\gamma)} &= \frac{1}{h_\beta}\left[\Delta S_2^{+(\beta\gamma)} - \Delta S_2^{-(\beta\gamma)}\right] \\ \Delta J_{3(00)}^{(\beta\gamma)} &= \frac{1}{l_\gamma}\left[\Delta S_3^{+(\beta\gamma)} - \Delta S_3^{-(\beta\gamma)}\right]\end{aligned} \tag{36}$$

With these definitions, the average of the incremental mass balance (13) yields:

$$\Delta J_{2(00)}^{(\beta\gamma)} + \Delta J_{3(000)}^{(\beta\gamma)} - \Delta\chi^{(\beta\gamma)} = 0 \tag{37}$$

where

$$\begin{aligned}\Delta\chi^{(\beta\gamma)} &= \frac{1}{h_\beta l_\gamma}\int_{-h_\beta}^{h_\beta}\int_{-l_\gamma}^{l_\gamma} [E_1\Delta\theta + E_2\Delta W]^{(\beta\gamma)}\, d\bar{Y}_2^{(\beta)} d\bar{Y}_3^{(\gamma)} \\ &= \Big\{E_1\Delta\theta_{(00)} + E_2\Big[H_{12}\Delta W_{1(10)} + H_{13}\Delta W_{1(01)} \\ &\quad + H_{22}\Delta W_{2(10)} + H_{23}\Delta W_{2(01)} + H_{32}\Delta W_{3(10)} + H_{33}\Delta W_{3(01)}\Big]\Big\}^{(\beta\gamma)}\end{aligned} \tag{38}$$

Thus,

$$\frac{1}{h_\beta}\left(\Delta S_2^{+(\beta\gamma)} - \Delta S_2^{-(\beta\gamma)}\right) + \frac{1}{l_\gamma}\left(\Delta S_3^{+(\beta\gamma)} - \Delta S_3^{-(\beta\gamma)}\right) - \Delta\chi^{(\beta\gamma)} = 0 \tag{39}$$

where

$$E_1^{(\beta\gamma)} = \frac{1}{1/\zeta^{(\beta\gamma)} + \epsilon}, \quad E_2^{(\beta\gamma)} = \left[\frac{\theta}{(1+\epsilon\zeta)^2}\frac{m}{\phi}\left(\frac{W}{\phi}\right)^{m-1}\zeta\right]^{(\beta\gamma)} \tag{40}$$

which are already known from the previous step.

Similarly to the increments in the surface-average tractions and mass fluxes as defined in Eqs. (26) and (35), the surface-average displacement increments can be defined by

$$\Delta\mathbf{U}_2^{\pm(\beta\gamma)} = \frac{1}{l_\gamma}\int_{-l_\gamma/2}^{l_\gamma/2} \Delta\mathbf{W}^{(\beta\gamma)}\left(\bar{Y}_2^{(\beta)} = \pm\frac{h_\beta}{2}\right) d\bar{Y}_3^{(\gamma)}$$

$$\Delta \mathbf{U}_3^{\pm(\beta\gamma)} = \frac{1}{h_\beta} \int_{-h_\beta/2}^{h_\beta/2} \Delta \mathbf{W}^{(\beta\gamma)} \left(\bar{Y}_3^{(\gamma)} = \pm \frac{l_\gamma}{2} \right) d\bar{Y}_2^{(\beta)} \tag{41}$$

In the following, the increments in the surface-average quantities, namely $\Delta \mathbf{U}_i^{\pm(\beta\gamma)}$, $i = 2, 3$, will be related to the microvariables increments $\mathbf{W}_{(mn)}^{(\beta\gamma)}$; $(mn) = 0, 1, 2$; as appear in the expansions (18). To this end, by substituting (18) into (41), the following relations are obtained:

$$\begin{aligned} \Delta \mathbf{U}_2^{\pm(\beta\gamma)} &= \Delta \mathbf{W}_{(00)}^{(\beta\gamma)} \pm \frac{h_\beta}{2} \Delta \mathbf{W}_{(10)}^{(\beta\gamma)} + \frac{h_\beta^2}{4} \Delta \mathbf{W}_{(20)}^{(\beta\gamma)} \\ \Delta \mathbf{U}_3^{\pm(\beta\gamma)} &= \Delta \mathbf{W}_{(00)}^{(\beta\gamma)} \pm \frac{l_\gamma}{2} \Delta \mathbf{W}_{(01)}^{(\beta\gamma)} + \frac{l_\gamma^2}{4} \Delta \mathbf{W}_{(02)}^{(\beta\gamma)} \end{aligned} \tag{42}$$

Manipulation of Eq. (42) by subtractions and additions yields

$$\begin{aligned} \Delta \mathbf{W}_{(10)}^{(\beta\gamma)} &= \frac{1}{h_\beta} \left[\Delta \mathbf{U}_2^{+} - \Delta \mathbf{U}_2^{-} \right]^{(\beta\gamma)} \\ \Delta \mathbf{W}_{(01)}^{(\beta\gamma)} &= \frac{1}{l_\gamma} \left[\Delta \mathbf{U}_3^{+} - \Delta \mathbf{U}_3^{-} \right]^{(\beta\gamma)} \end{aligned} \tag{43}$$

and

$$\begin{aligned} \Delta \mathbf{W}_{(20)}^{(\beta\gamma)} &= \frac{2}{h_\beta^2} \left[\Delta \mathbf{U}_2^{+} + \Delta \mathbf{U}_2^{-} \right]^{(\beta\gamma)} - \frac{4}{h_\beta^2} \Delta \mathbf{W}_{(00)}^{(\beta\gamma)} \\ \Delta \mathbf{W}_{(02)}^{(\beta\gamma)} &= \frac{2}{l_\gamma^2} \left[\Delta \mathbf{U}_3^{+} + \Delta \mathbf{U}_3^{-} \right]^{(\beta\gamma)} - \frac{4}{l_\gamma^2} \Delta \mathbf{W}_{(00)}^{(\beta\gamma)} \end{aligned} \tag{44}$$

Similarly, we define:

$$\begin{aligned} \Delta \theta_2^{\pm(\beta\gamma)} &= \frac{1}{l_\gamma} \int_{-l_\gamma/2}^{l_\gamma/2} \Delta \theta^{(\beta\gamma)} \left(\bar{Y}_2^{(\beta)} = \pm \frac{h_\beta}{2} \right) d\bar{Y}_3^{(\gamma)} \\ \Delta \theta_3^{\pm(\beta\gamma)} &= \frac{1}{h_\beta} \int_{-h_\beta/2}^{h_\beta/2} \Delta \theta^{(\beta\gamma)} \left(\bar{Y}_3^{(\gamma)} = \pm \frac{l_\gamma}{2} \right) d\bar{Y}_2^{(\beta)} \end{aligned} \tag{45}$$

By employing the expansion of $\Delta\theta$ in Eq. (19), we obtain:

$$\begin{aligned} \Delta \theta_2^{\pm(\beta\gamma)} &= \Delta \theta_{(00)}^{(\beta\gamma)} \pm \frac{h_\beta}{2} \Delta \theta_{(10)}^{(\beta\gamma)} + \frac{h_\beta^2}{4} \Delta \theta_{(20)}^{(\beta\gamma)} \\ \Delta \theta_3^{\pm(\beta\gamma)} &= \Delta \theta_{(00)}^{(\beta\gamma)} \pm \frac{l_\gamma}{2} \Delta \theta_{(01)}^{(\beta\gamma)} + \frac{l_\gamma^2}{4} \Delta \theta_{(02)}^{(\beta\gamma)} \end{aligned} \tag{46}$$

Manipulation of Eq. (46) by subtractions and additions yields

$$\begin{aligned} \Delta \theta_{(10)}^{(\beta\gamma)} &= \frac{1}{h_\beta} \left[\Delta \theta_2^{+} - \Delta \theta_2^{-} \right]^{(\beta\gamma)} \\ \Delta \theta_{(01)}^{(\beta\gamma)} &= \frac{1}{l_\gamma} \left[\Delta \theta_3^{+} - \Delta \theta_3^{-} \right]^{(\beta\gamma)} \end{aligned} \tag{47}$$

and

$$\begin{aligned} \Delta \theta_{(20)}^{(\beta\gamma)} &= \frac{2}{h_\beta^2} \left[\Delta \theta_2^{+} + \Delta \theta_2^{-} \right]^{(\beta\gamma)} - \frac{4}{h_\beta^2} \Delta \theta_{(00)}^{(\beta\gamma)} \\ \Delta \theta_{(02)}^{(\beta\gamma)} &= \frac{2}{l_\gamma^2} \left[\Delta \theta_3^{+} + \Delta \theta_3^{-} \right]^{(\beta\gamma)} - \frac{4}{l_\gamma^2} \Delta \theta_{(00)}^{(\beta\gamma)} \end{aligned} \tag{48}$$

It is now possible to express $\Delta\mathbf{W}_{(00)}^{(\beta\gamma)}$ in terms of the surface-average displacement increments $\Delta\mathbf{U}_i^{\pm(\beta\gamma)}$; $i = 2, 3$. This is achieved by substituting Eqs. (43)–(44) in Eqs. (32)–(34). As a result, a system of three linear algebraic equations in the three unknowns $\Delta\mathbf{W}_{(00)}^{(\beta\gamma)}$ is obtained. The solution of this system of equations expresses the aforementioned microvariables in terms of $\Delta\mathbf{U}_i^{\pm(\beta\gamma)}$ and $\Delta\theta_i^{\pm(\beta\gamma)}$, i=2,3.

As for $\Delta\theta_{(00)}^{(\beta\gamma)}$, it can be determined by substituting Eqs. (47) and (48) in the incremental mass balance (37). Hence these solutions, along with Eqs. (43)–(44) and (47)–(48), can be represented as follows:

$$\begin{Bmatrix} \Delta\mathbf{W}_{(00)} \\ \Delta\mathbf{W}_{(10)} \\ \Delta\mathbf{W}_{(01)} \\ \Delta\mathbf{W}_{(20)} \\ \Delta\mathbf{W}_{(02)} \\ \Delta\theta_{(00)} \\ \Delta\theta_{(10)} \\ \Delta\theta_{(01)} \\ \Delta\theta_{(20)} \\ \Delta\theta_{(02)} \end{Bmatrix}^{(\beta\gamma)} = \mathbf{M}^{(\beta\gamma)} \begin{Bmatrix} \Delta\mathbf{U}_2^+ - \Delta\mathbf{U}_2^- \\ \Delta\mathbf{U}_3^+ - \Delta\mathbf{U}_3^- \\ \Delta\theta_2^+ - \Delta\theta_2^- \\ \Delta\theta_3^+ - \Delta\theta_3^- \end{Bmatrix}^{(\beta\gamma)} \tag{49}$$

where $\mathbf{M}_i^{(\beta\gamma)}$ are matrices whose elements are quite cumbersome and hence are omitted here.

Consequently, with expressions (49), the following relations can be established from Eqs. (29)–(30):

$$\begin{Bmatrix} \Delta\mathbf{T}_2^{\pm} \\ \Delta\mathbf{T}_3^{\pm} \\ \Delta S_2^{\pm} \\ \Delta S_3^{\pm} \end{Bmatrix}^{(\beta\gamma)} = \mathbf{K}^{(\beta\gamma)} \begin{Bmatrix} \Delta\mathbf{U}_2^{\pm} \\ \Delta\mathbf{U}_3^{\pm} \\ \Delta\theta_2^{\pm} \\ \Delta\theta_3^{\pm} \end{Bmatrix}^{(\beta\gamma)} + \begin{Bmatrix} \Delta\mathbf{\Phi}_2^{\pm} \\ \Delta\mathbf{\Phi}_3^{\pm} \\ 0 \\ 0 \end{Bmatrix}^{(\beta\gamma)} \tag{50}$$

where $\mathbf{K}^{(\beta\gamma)}$ is a square matrix of the 16th-order which consists of the instantaneous properties $\mathbf{Z}^{(\beta\gamma)}$ of the material filling subcell $(\beta\gamma)$, and its geometric dimensions. In these equations, the vectors $\Delta\mathbf{\Phi}_i^{\pm(\beta\gamma)}$, $i = 2, 3$, are the far-field contributions. Those are defined by:

$$\begin{aligned} \Delta\mathbf{\Phi}_2^{\pm(\beta\gamma)} &= \left[\sum_{p=1}^{9} Z_{4p}^{(\beta\gamma)} \Delta\bar{\Omega}_p, \quad \sum_{p=1}^{9} Z_{5p}^{(\beta\gamma)} \Delta\bar{\Omega}_p, \quad \sum_{p=1}^{9} Z_{6p}^{(\beta\gamma)} \Delta\bar{\Omega}_p \right] \\ \Delta\mathbf{\Phi}_3^{\pm(\beta\gamma)} &= \left[\sum_{p=1}^{9} Z_{7p}^{(\beta\gamma)} \Delta\bar{\Omega}_p, \quad \sum_{p=1}^{9} Z_{8p}^{(\beta\gamma)} \Delta\bar{\Omega}_p, \quad \sum_{p=1}^{9} Z_{9p}^{(\beta\gamma)} \Delta\bar{\Omega}_p \right] \end{aligned} \tag{51}$$

The continuity conditions of the surface-averaged displacement and the surface-averaged traction increments between neighboring subcells require that

$$\begin{aligned} [\Delta\mathbf{U}_2 \quad \Delta\mathbf{T}_2]^{+(\beta\gamma)} &= [\Delta\mathbf{U}_2 \quad \Delta\mathbf{T}_2]^{-(\beta+1\,\gamma)}, \quad \beta = 1, ..., N_\beta - 1, \ \gamma = 1, ..., N_\gamma \\ [\Delta\mathbf{U}_3 \quad \Delta\mathbf{T}_3]^{+(\beta\gamma)} &= [\Delta\mathbf{U}_3 \quad \Delta\mathbf{T}_3]^{-(\beta\,\gamma+1)}, \quad \beta = 1, ..., N_\beta, \ \gamma = 1, ..., N_\gamma - 1 \end{aligned} \tag{52}$$

In addition, one has

$$\begin{aligned} [\Delta\theta_2 \quad \Delta S_2]^{+(\beta\gamma)} &= [\Delta\theta_2 \quad \Delta S_2]^{-(\beta+1\,\gamma)}, \quad \beta = 1, ..., N_\beta - 1, \ \gamma = 1, ..., N_\gamma \\ [\Delta\theta_3 \quad \Delta S_3]^{+(\beta\gamma)} &= [\Delta\theta_3 \quad \Delta S_3]^{-(\beta\,\gamma+1)}, \quad \beta = 1, ..., N_\beta, \ \gamma = 1, ..., N_\gamma - 1 \end{aligned} \tag{53}$$

Next, the periodicity conditions that require the equality of the surface-averaged displacement increments as well as the surface-averaged traction increments at the opposite sides of the RUC read

$$\begin{aligned} [\Delta\mathbf{U}_2 \quad \Delta\mathbf{T}_2]^{-(1\gamma)} &= [\Delta\mathbf{U}_2 \quad \Delta\mathbf{T}_2]^{+(N_\beta\,\gamma)}, \quad \gamma = 1, ..., N_\gamma \\ [\Delta\mathbf{U}_3 \quad \Delta\mathbf{T}_3]^{-(\beta 1)} &= [\Delta\mathbf{U}_3 \quad \Delta\mathbf{T}_3]^{+(\beta\,N_\gamma)}, \quad \beta = 1, ..., N_\beta \end{aligned} \tag{54}$$

and

$$\begin{aligned}
[\Delta\theta_2 \quad \Delta S_2]^{-(1\gamma)} &= [\Delta\theta_2 \quad \Delta S_2]^{+(N_\beta\ \gamma)}, \quad \gamma = 1, ..., N_\gamma \\
[\Delta\theta_3 \quad \Delta S_3]^{-(\beta 1)} &= [\Delta\theta_3 \quad \Delta S_3]^{+(\beta\ N_\gamma)}, \quad \beta = 1, ..., N_\beta
\end{aligned} \tag{55}$$

Equations (52)–(55) form a system of $16N_\beta N_\gamma$ algebraic equations of the same number as that of the surface-averaged displacement increments $\Delta\mathbf{U}_2^{\pm(\beta\gamma)}$, $\Delta\mathbf{U}_3^{\pm(\beta\gamma)}$ together with the surface-averaged increments $\Delta\theta_2^{\pm(\beta\gamma)}$, $\Delta\theta_3^{\pm(\beta\gamma)}$ in all the subcells of the RUC (the composite). This system can be represented as:

$$\begin{bmatrix} \mathbf{A}_{11} & \mathbf{A}_{12} \\ \mathbf{A}_{21} & \mathbf{A}_{22} \end{bmatrix} \begin{Bmatrix} \Delta\mathbf{U}^{\pm} \\ \Delta\boldsymbol{\theta}^{\pm} \end{Bmatrix} = \begin{bmatrix} \Delta\boldsymbol{\Phi}^{\pm}(\Delta\bar{\mathbf{F}}) \\ \mathbf{0} \end{bmatrix} \tag{56}$$

where $\Delta\boldsymbol{\Phi}^{\pm}$ denotes the applied far-field mechanical increments.

4 Method of solution

Attempts to solve for the coupled mechanical and intact material mass fraction fields, as represented by Eq. (56), simultaneously, fail. To resolve this, a predictor–corrector approach is implemented, as discussed in the following. The physical understanding behind the predictor–corrector split is that bond rupture and deformation of the continuum occur on different time scales. Damage can either occur very quickly, under fixed deformation, or be practically constant during the deformation of the continuum. In either case, there is separation of time scales, calling for a two- or three-step scheme. One can first assume a change in stress under fixed level of damage (that already occurred), then damage evolution under a fixed deformation level, and then again a deformation step under fixed damage level, assumed to take place after the subsequent quantum of damage has occurred. This understanding underlies also the predictor–corrector scheme as proposed by Hofacker and Miehe [17].

Let Eq. (50) be represented in the form

$$\begin{Bmatrix} \Delta\mathbf{T} \\ \Delta\mathbf{S} \end{Bmatrix}^{(\beta\gamma)} = \begin{bmatrix} \mathbf{K}_{11} & \mathbf{K}_{12} \\ \mathbf{K}_{21} & \mathbf{K}_{22} \end{bmatrix}^{(\beta\gamma)} \begin{Bmatrix} \Delta\mathbf{U} \\ \Delta\boldsymbol{\theta} \end{Bmatrix}^{(\beta\gamma)} + \begin{Bmatrix} \Delta\boldsymbol{\Phi} \\ 0 \end{Bmatrix}^{(\beta\gamma)} \tag{57}$$

Instead of imposing the continuity and periodicity conditions (52)–(55) to form the global coupled Eq. (56), the following three predictor/corrector problems are introduced.

Problem I: Here, the following modified relations are used instead of Eq. (57):

$$\{\Delta\mathbf{T}\}^{(\beta\gamma)} = [\mathbf{K}_{11}]^{(\beta\gamma)} \{\Delta\hat{\mathbf{U}}\}^{(\beta\gamma)} + \{\Delta\boldsymbol{\Phi}\}^{(\beta\gamma)} \tag{58}$$

Imposing the continuity and periodicity conditions (52)–(55) results in a global system of equations providing $\Delta\hat{\mathbf{U}}^{(\beta\gamma)}$ in all the subcells.

Problem II: In the framework of this problem, Eq. (57) is modified to include the established increments $\Delta\hat{\mathbf{U}}^{(\beta\gamma)}$, as follows:

$$\{\Delta\mathbf{S}\}^{(\beta\gamma)} = [\mathbf{K}_{22}]^{(\beta\gamma)} \{\Delta\boldsymbol{\theta}\}^{(\beta\gamma)} + \{\mathbf{K}_{21}\Delta\hat{\mathbf{U}}\}^{(\beta\gamma)} \tag{59}$$

By implementing the continuity and periodicity conditions (52)–(55), the solution of the resulting global equation yields $\Delta\boldsymbol{\theta}^{(\beta\gamma)}$ in all the subcells. Consequently, the mass fractions in all the subcells can be determined according to

$$\boldsymbol{\theta}^{(\beta\gamma)} = \boldsymbol{\theta}^{(\beta\gamma)}_{\text{previous}} + \Delta\boldsymbol{\theta}^{(\beta\gamma)} \tag{60}$$

where $\boldsymbol{\theta}^{(\beta\gamma)}_{\text{previous}}$ is the mass fractions that were computed at the previous applied loading increment.

Figures 14 and 15 show the case of a MY material with randomly positioned identical BK fibers. This case may be representative of fiber-strengthening of aortic fabric.

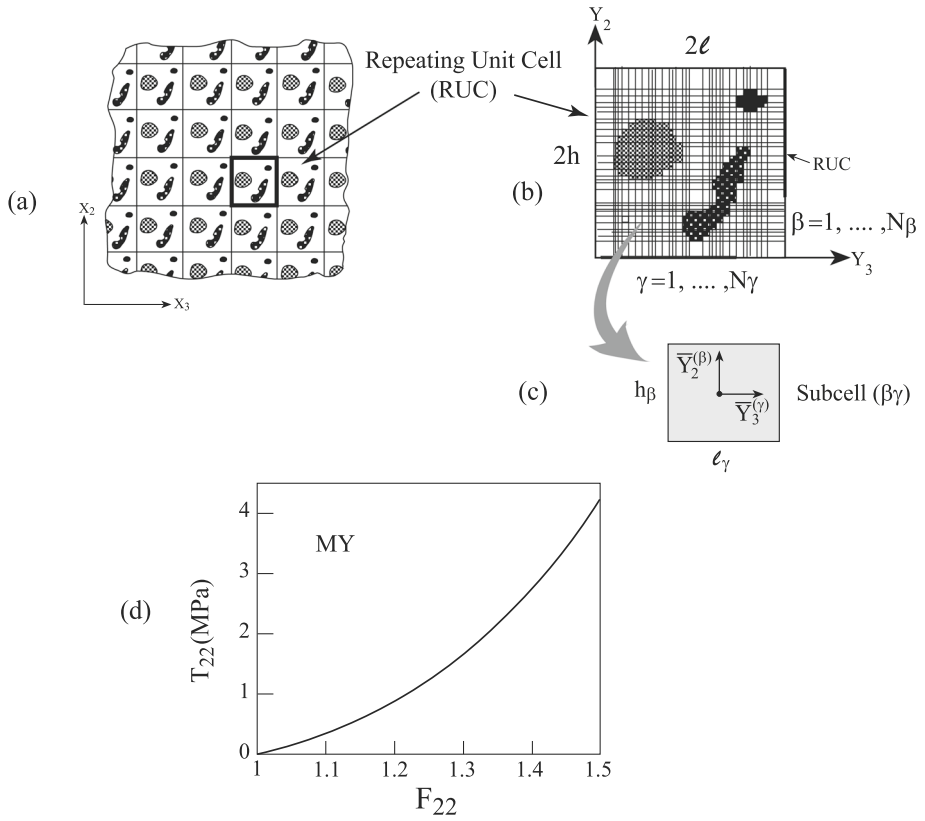

Fig. 1 **a** A doubly periodic composite, defined with respect to global initial coordinates (X_1, X_2, X_3). **b** A repeating unit cell (RUC), represented with respect to local initial coordinates (Y_1, Y_2, Y_3). It is divided into N_β and N_γ subcells, in the Y_2 and Y_3 directions, respectively. **c** A characteristic subcell $(\beta\gamma)$ with initial local coordinates $\bar{Y}_2^{(\beta)}$ and $\bar{Y}_3^{(\gamma)}$ whose origin is located at its center. **d** The uniaxial stress response of the material characterized by the assumed hyperelastic strain energy function (67)

Problem III: With the computed mass fractions $\boldsymbol{\theta}^{(\beta\gamma)}$ in all the subcells, the following modification of Eq. (57) is used:

$$\left\{\Delta\mathbf{T}\right\}^{(\beta\gamma)} = \left[\mathbf{K}_{11}\right]^{(\beta\gamma)} \left\{\Delta\mathbf{U}\right\}^{(\beta\gamma)} + \left\{\Delta\boldsymbol{\Phi} + \mathbf{K}_{12}\Delta\boldsymbol{\theta}\right\}^{(\beta\gamma)} \tag{61}$$

Imposing the continuity and periodicity conditions (52)–(55) yields a global equation whose solution provides $\Delta\mathbf{U}^{(\beta\gamma)}$ in all the subcells. Hence,

$$\mathbf{U}^{(\beta\gamma)} = \mathbf{U}^{(\beta\gamma)}_{\text{previous}} + \Delta\mathbf{U}^{(\beta\gamma)} \tag{62}$$

From Eq. (49), it is evident that the mechanical and mass fraction increments $\Delta W_{mn}^{(\beta\gamma)}$ and $\Delta\theta_{mn}^{(\beta\gamma)}$; $m = n = 0, 1, 2$ can be considered determined in all the subcells.

The solution provides, in particular, the concentration matrices $\mathbf{C}^{(\beta\gamma)}$, which relate the increments in the local displacement gradients $\Delta\mathbf{F}^{(\beta\gamma)}$ and the mass fraction $\Delta\theta^{(\beta\gamma)}$ in the subcell, to the externally applied mechanical loading increment, $\Delta\bar{\mathbf{F}}$:

$$\left\{\begin{array}{c}\Delta\mathbf{F}\\ \Delta\theta\end{array}\right\}^{(\beta\gamma)} = \mathbf{C}^{(\beta\gamma)}\Delta\bar{\mathbf{F}} \tag{63}$$

where it should be noted that $\mathbf{C}^{(\beta\gamma)}$ is a 10×9 rectangular matrix.

By substitution of $\Delta\mathbf{F}^{(\beta\gamma)}$ and $\Delta\theta^{(\beta\gamma)}$ into Eq. (7) of subcell $(\beta\gamma)$, the following equation is obtained:

$$\Delta\boldsymbol{\Sigma}^{(\beta\gamma)} = \hat{\mathbf{Z}}^{(\beta\gamma)}\Delta\bar{\mathbf{F}} \tag{64}$$

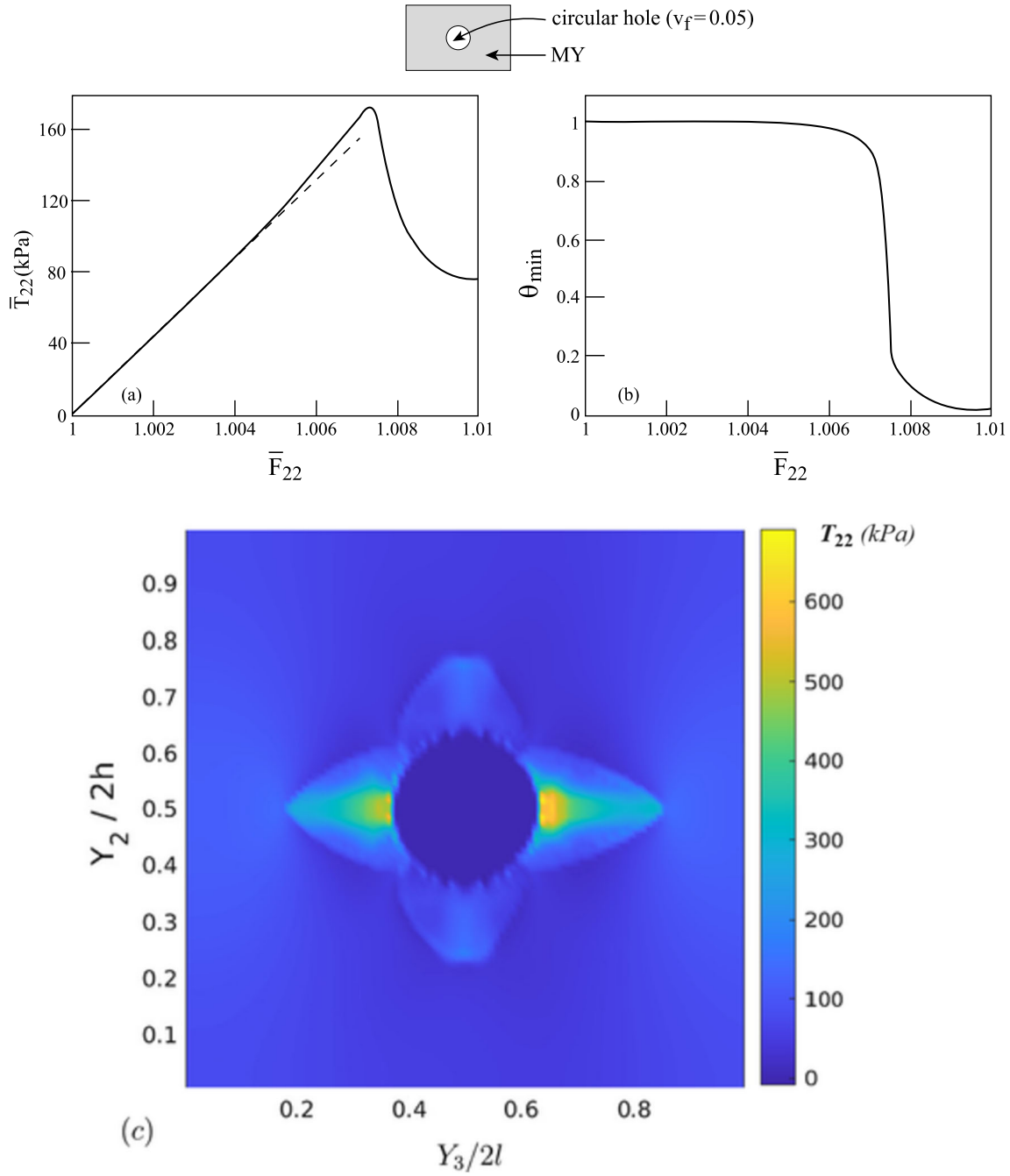

Fig. 2 A composite with a circular hole of $v_f = 0.05$ porosity. **a** Global response $\bar{T}_{22} - \bar{F}_{22}$. **b** Plot of $\theta_{\min}$ against $\bar{F}_{22}$. **c** Stress (T_{22}) distribution

where $\hat{\mathbf{Z}}^{(\beta\gamma)}$ is a ninth-order square matrix, the elements of which are given in terms of $\mathbf{C}^{(\beta\gamma)}$, $\mathbf{Z}^{(\beta\gamma)}$ and $\mathbf{H}^{(\beta\gamma)}$.

By averaging the stress increments $\Delta\mathbf{T}^{(\beta\gamma)}$ over all the subcells of the RUC, the following relation, governing the global response of the composite, is established:

$$\Delta\bar{\boldsymbol{\Sigma}} = \mathbf{Z}^{*}\Delta\bar{\mathbf{F}} \tag{65}$$

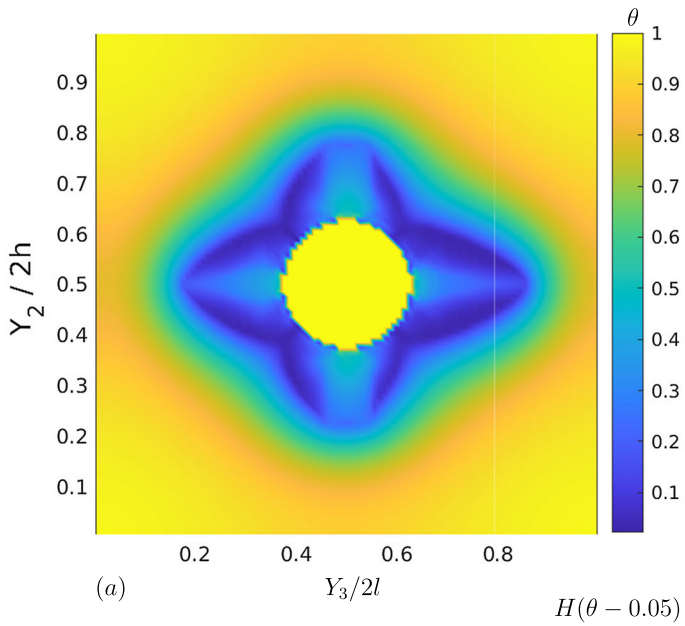

Fig. 3 **a** Intact mass fraction θ distribution. **b** Intact mass fraction θ distribution—binary pivot at 0.05

The effective first tangent $\mathbf{Z}^*$ of the composite is then given by

$$\mathbf{Z}^* = \frac{1}{4hl} \sum_{\beta=1}^{N_\beta} \sum_{\gamma=1}^{N_\gamma} h_\beta l_\gamma \hat{\mathbf{Z}}^{(\beta\gamma)} \tag{66}$$

5 Applications

Example results for the offered analysis are obtained by choosing the following hyperelastic energy W, which is referred to as the modified Yeoh energy function:

$$W = C_1 \left(\hat{I}_1 - 3\right) + C_2 \left(\hat{I}_1 - 3\right)^2 + \frac{K}{2} (J-1)^2 \tag{67}$$

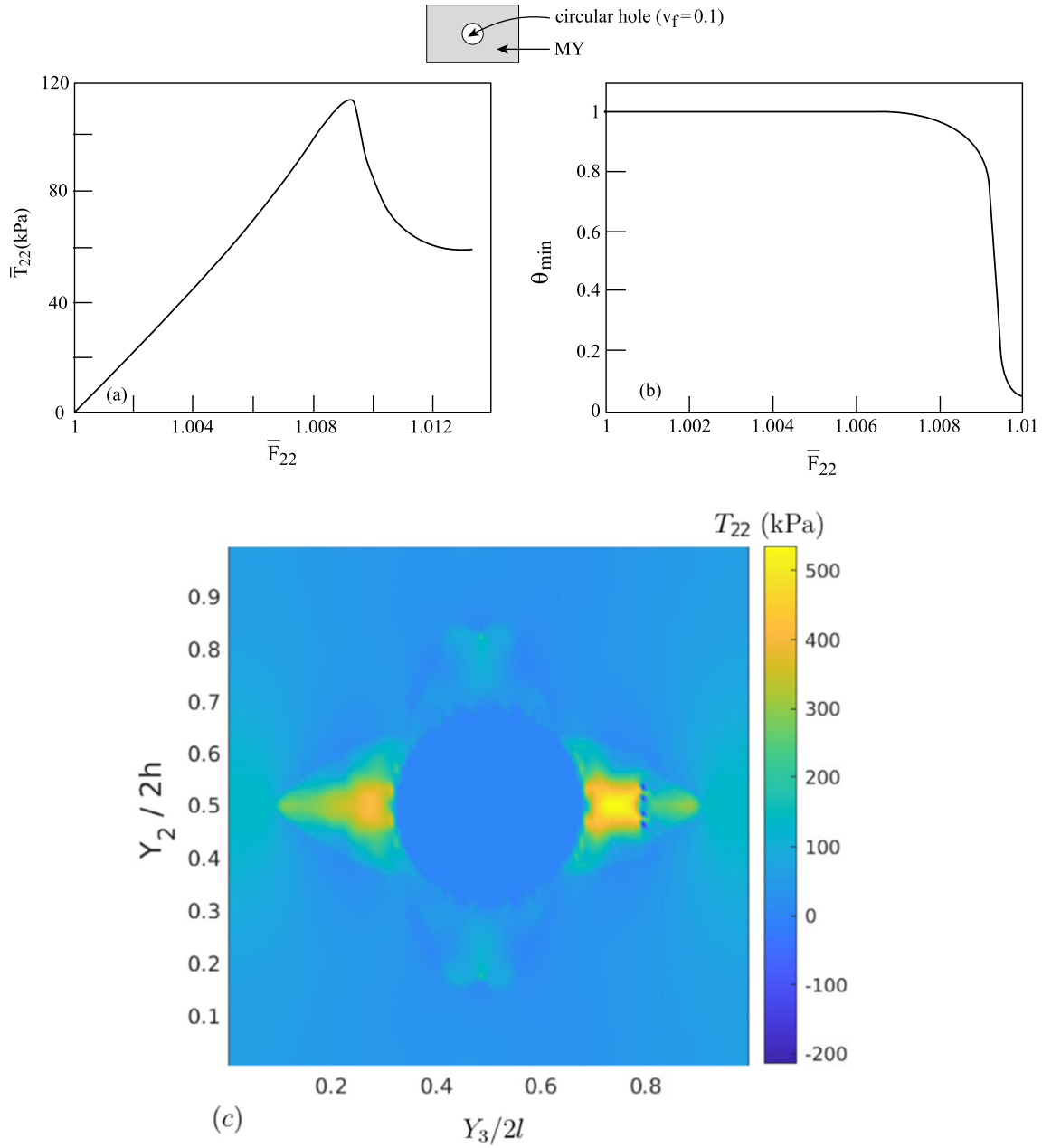

Fig. 4 A composite with a circular hole of $v_f = 0.1$ porosity. **a** Global response $\bar{T}_{22} - \bar{F}_{22}$. **b** Plot of $\theta_{\min}$ against $\bar{F}_{22}$. **c** Stress (T_{22}) distribution

where $\hat{I}_1 = I_1/J^{2/3}$, $I_1 = F_{ij}F_{ij}$, $J = det\ \mathbf{F}$ and C_1, C_2, K are material constants. The following values are used: $C_1 = 0.617$ MPa, $C_2 = 1.215$ MPa, K = 0.5 GPa, $\phi = 0.1686$ MPa, $\bar{l} = 0.1$mm, $m = 3$. The size of the RUC is $2h = 2l = 1$ mm, and it is divided into $N_\beta N_\gamma$ subcells with $N_\beta = N_\gamma = 100$.

For the cases where a composite, rather than porous material is addressed, the second phase is modeled by the Blatz and Ko material, (see Blatz and Ko [7]):

$$W = \frac{\mu}{2}\left(\frac{I_2}{I_3} + 2\sqrt{I_3} - 5\right) \tag{68}$$

where I_2 and I_3 are the second invariant and the determinant of the right Cauchy–Green deformation tensor $\mathbf{C} = \mathbf{F}^T\mathbf{F}$, respectively, with $\mu = 0.22$ MPa.

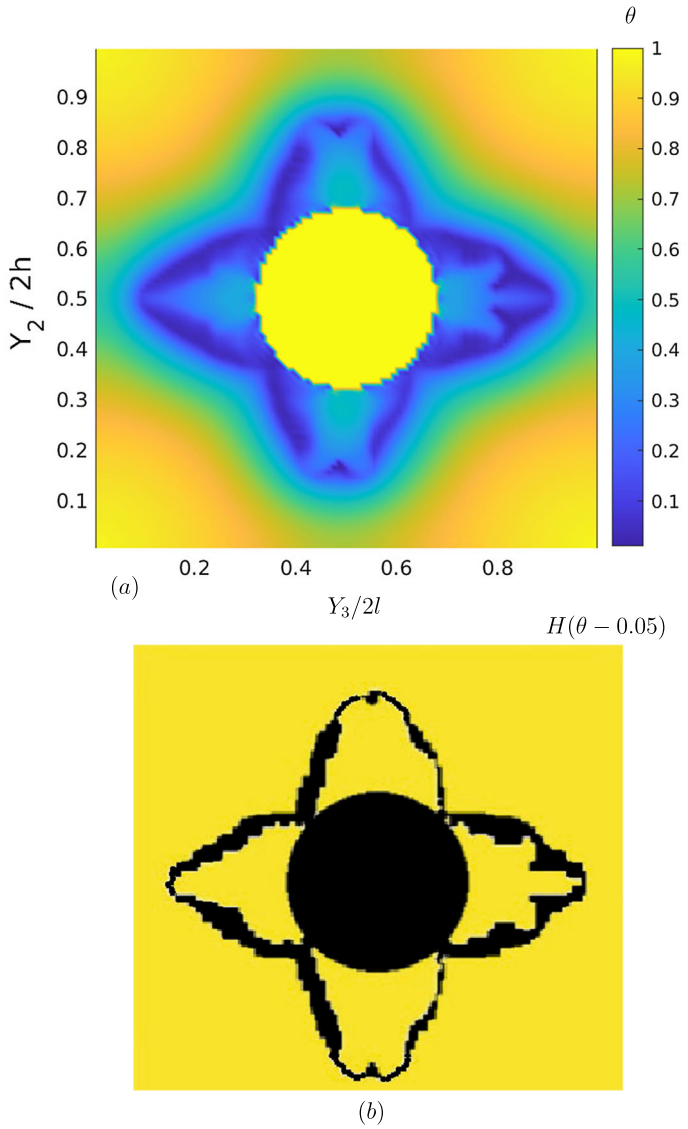

Fig. 5 **a** Intact mass fraction θ distribution. **b** Intact mass fraction θ distribution—binary pivot at 0.05

6 Discussion of the results

Figure 1 shows a typical composite, with the repeating unit cell, a rectangular grid of computational subcells and the coordinate system inside a subcell. Figure 1d shows the hyperelastic (convex) response of a modified Yeoh (MY) material.

Figure 2 shows the first examined case of material with a circular cavity of 5% volume (area), and the corresponding stress–deformation curve, which exhibits superlinear behavior up to a maximum value, after which convex decrease is observed. The response is similar to the one reported in Dean et al. [12], Bui and Hu [11] and Denli et al. [13]. The second plot presents the decrease in the spatial minimum of the intact material ratio θ with applied far-field deformation, showing a sharp dependence typical for brittle fracture in a smooth description. Figure 2c shows the expected stress concentration by the sides of a cavity in vertical stretch.

Figure 3a, b shows the damage pattern in the form of four cracks running at 45° to the principal axes and splitting to two cracks each with branch-like form.

Figures 4 and 5 show the result for a case similar to the one in Fig. 2, but when the circular cavity comprises 10% of the volume. Figure 5b shows a sharpened pattern of θ (in black when it is above 0.05), showing an interesting phenomenon appearing as coalescence of cracks.

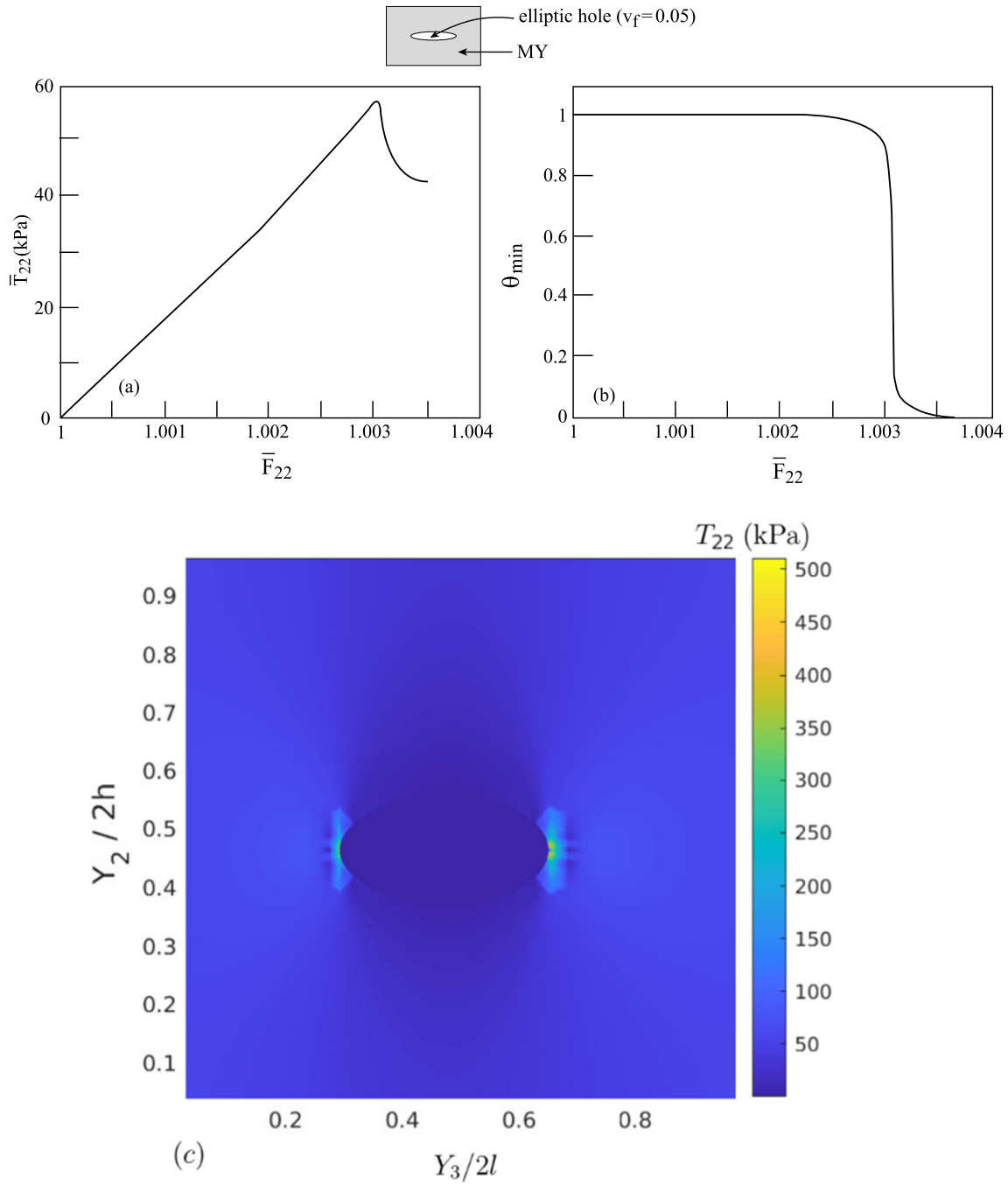

Fig. 6 A composite with an elliptic hole (ratio of major to minor axis is 2) of $v_f = 0.05$ porosity. **a** Global response $\bar{T}_{22} - \bar{F}_{22}$. **b** Plot of $\theta_{\min}$ against $\bar{F}_{22}$. **c** Stress (T_{22}) distribution

Figures 6, 7, 8 and 9 show the cases where the cavity is of elliptical cross section, either horizontally or vertically aligned, with plots and color maps as one could expect.

Figures 10 and 11 show the scenario of a cylindrical inclusion made of Blatz–Ko (BK) material in a matrix made of a modified Yeoh material (MY). Since BK material is less stiff than MY material, the results are qualitatively similar to those shown in Fig. 2.

Figures 12 and 13 address the opposite case, of a matrix made of BK material and an inclusion made of a MY material. Interestingly enough, decrease in stress is not observed here even for 10% strain, since the matrix

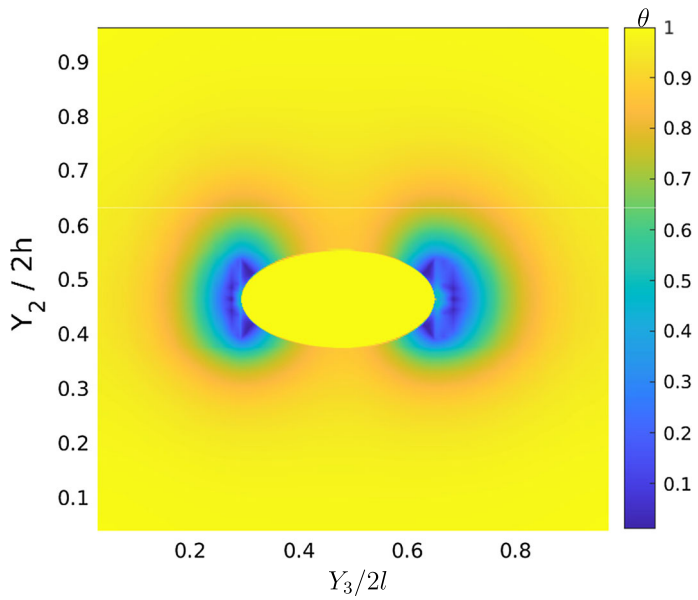

Fig. 7 Intact mass fraction θ distribution for a horizontal elliptic inclusion

takes on most of the force and it does not develop damage. Nevertheless, θ decreases to zero at the damage loci, which, much like the stress concentration zones, are developing along the vertical axis (contrary to the case with a cavity and a MY matrix, where for vertical loading stress concentration loci lie on the horizontal axis). Moreover, the stress and damage concentration zones do not develop on the axis of symmetry. Rather, there seems to be symmetry breaking here, typical for nonlinear response with a spinodal part. (Here, the spinodal is in the MY material, since the BK material is convex.)

The stress map in Fig. 12c shows expected stress concentration zones in the MY material inclusions close to the damage loci shown in Fig 13.

For this case, the stress–deformation response is interestingly sublinear even before the maximum stress is reached, with a typical drop after the maximum. Figure 15b shows the θ map, where apparently the low-θ zones concentrate around the corners of the unit cell.

It should be noted here that the case of a BK matrix exhibits strong symmetry breaking that can be attributed to the instability characteristic for nonlinear composites with a compliant matrix and a stiffer inclusion undergoing gradual damage. Strong symmetry breaking is also observed in the case of random distribution of BK fibers, as shown in Fig. 15, and is not unexpected. One might wonder regarding the adequacy of periodic boundary conditions for the case of a random pattern of inclusions in a matrix. Periodic boundary conditions imply that the distribution of the stress and damage fields inside a representative unit cell is expected to be the same for all the cells. This can only hold if the cells have identical distribution of fibers, even if it is a random one. The present approach is designed specifically for the analysis of periodic composites, not random ones. Thus, it is not opted here to analyze an infinite span of random composite matter. Instead, it is assumed that the material is periodic, with identical cells, where the representative cell has a random distribution of inclusions, perhaps as a result of some topology optimization procedure for desired response, and the representative cells are glued to a periodic pattern. In such a setting, the fibers will be of non-circular cross section at the boundaries of the unit cells. Moreover, the adhesive layers required for practical implementations are neglected here. It is also possible to maintain the picture of right fibers by modeling only a quarter of the RUC as random and reflecting it in both directions. However, the level of randomness of that pattern will be smaller than that of the chosen pattern. It is also possible to position all the inclusions well inside the unit cell, to prevent an inclusion from having a non-circular cross section; however, it is only crucial for rigid authentic fibers, such as those made of carbon or glass. In the examined case, the inclusion modeled by a BK material was needed only to model a different phase, with no damage accumulation and the circular cross section is not a rigid requirement. A random unit cell made with BK fibers can be cut from a larger random pattern, with some fibers cut in the middle. Then, a periodic pattern can be constructed from gluing the unit cells together. With some fibers cut in the middle, an even more random pattern is reproduced, albeit with periodicity on the macro-scale. The main

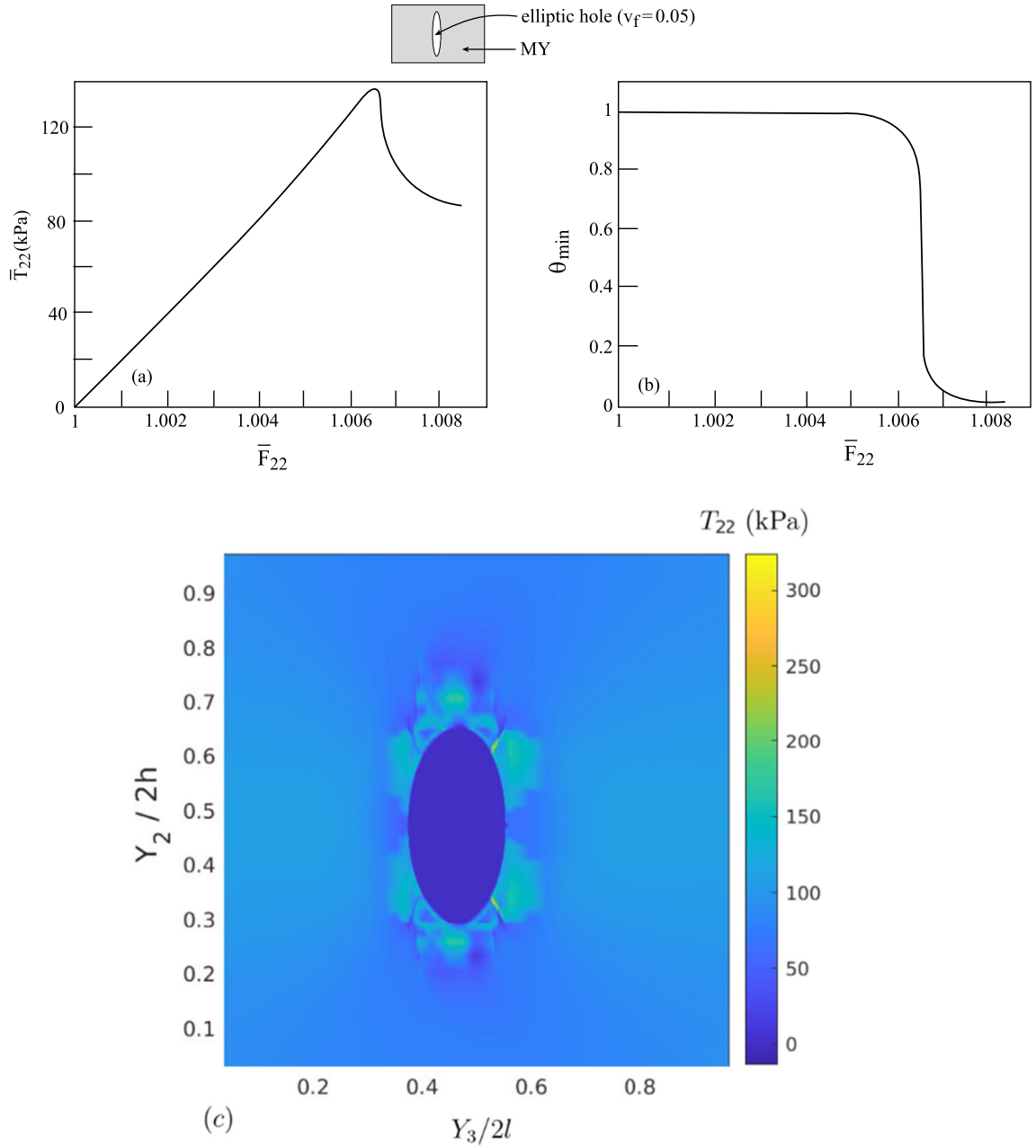

Fig. 8 A composite with an elliptic hole (ratio of major to minor axis is 1/2 of $v_f = 0.05$ porosity. **a** Global response $\bar{T}_{22} - \bar{F}_{22}$. **b** Plot of $\theta_{\min}$ against $\bar{F}_{22}$. **c** Stress (T_{22}) distribution

point in the analysis of the random pattern is in any case to observe the spontaneous localization of damage based on the intricacies of non-trivial stress localization geometry.

An important remark should be made at this point. Damage nucleation is in principle an instability-related phenomenon, and as such it is expected to exhibit spatial localization. In Breiman et al. [10], the spatially homogeneous case was addressed. In the present work, spatial localization is enabled inside the representative unit cell; however, periodicity is maintained between the different cells. In a more realistic scenario, even small variation (between the cells) in material parameters related to damage is expected to lead to periodicity-breaking and localization of damage in a specific cell. This case of localization in a two-scale modeling can be addressed in the manner discussed in Perchikov and Aboudi [21], albeit with evolving damage, rather than fixed one, as assumed therein. Such generalization of the present study to the case of damage localization on the scale of

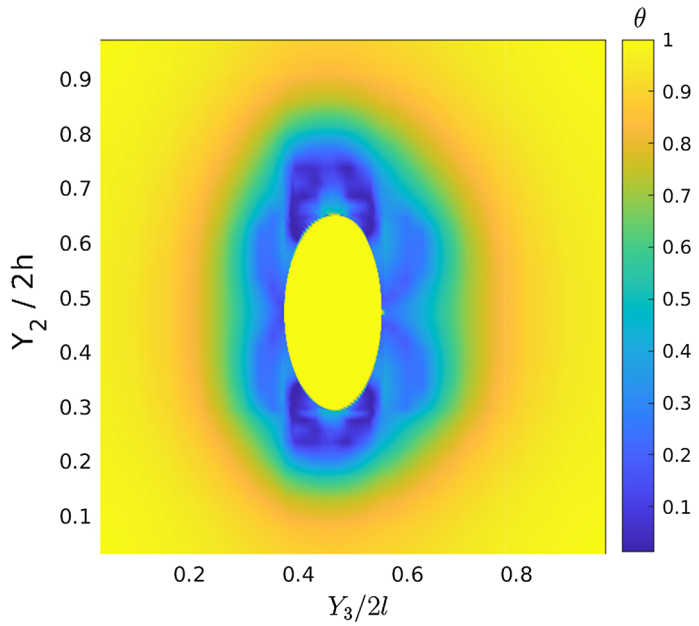

Fig. 9 Intact mass fraction θ distribution for a vertical elliptic inclusion

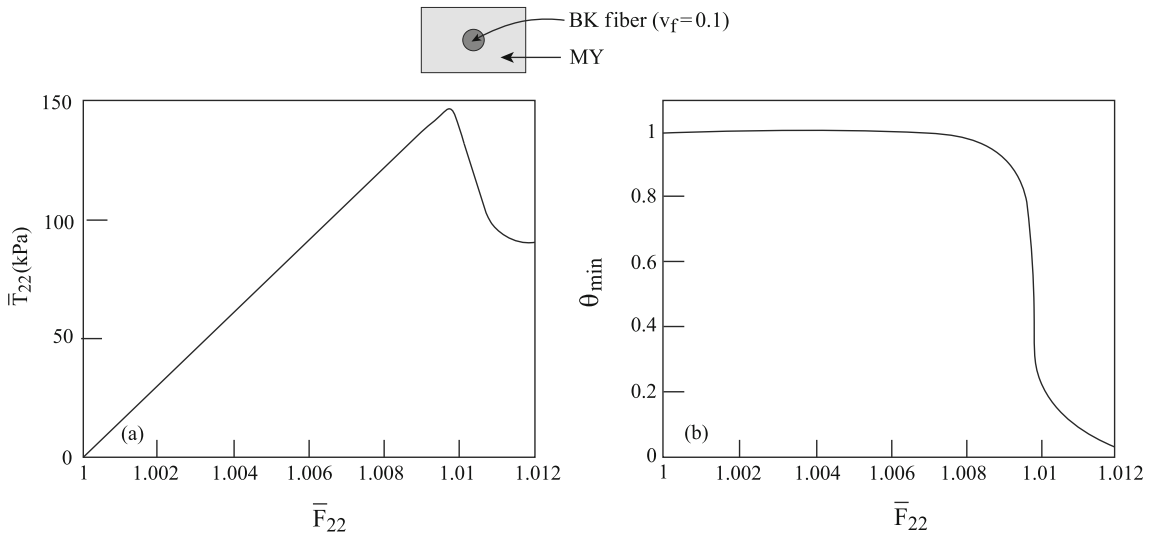

Fig. 10 A BK/modified Yeoh composite with a circular fiber of $v_f = 0.1$ fiber volume fraction. **a** Global response $\bar{T}_{22} - \bar{F}_{22}$. **b** Plot of $\theta_{\min}$ against $\bar{F}_{22}$

the representative unit cells will be addressed by the authors in subsequent work. In the present formulation, the periodicity of damage is assumed to be representative of perfect periodicity in material properties between the cells, preventing large-scale physical damage localization instability from being manifested.

7 Conclusions

In this work, the finite strain high-fidelity general method of cells was extended to treat micromechanics of a composite, one of the phases in which undergoes gradual mechanical degradation, in the form of crumbling of initially intact hyperelastic material. The damage depends strongly on the stress, in a smoothed threshold-like fashion, which leads to effective formation of crack-like damaged regions. Mathematically, the equation governing the evolution of damage is nonlocal and two-way coupled to stress (or rather, energy density), somewhat

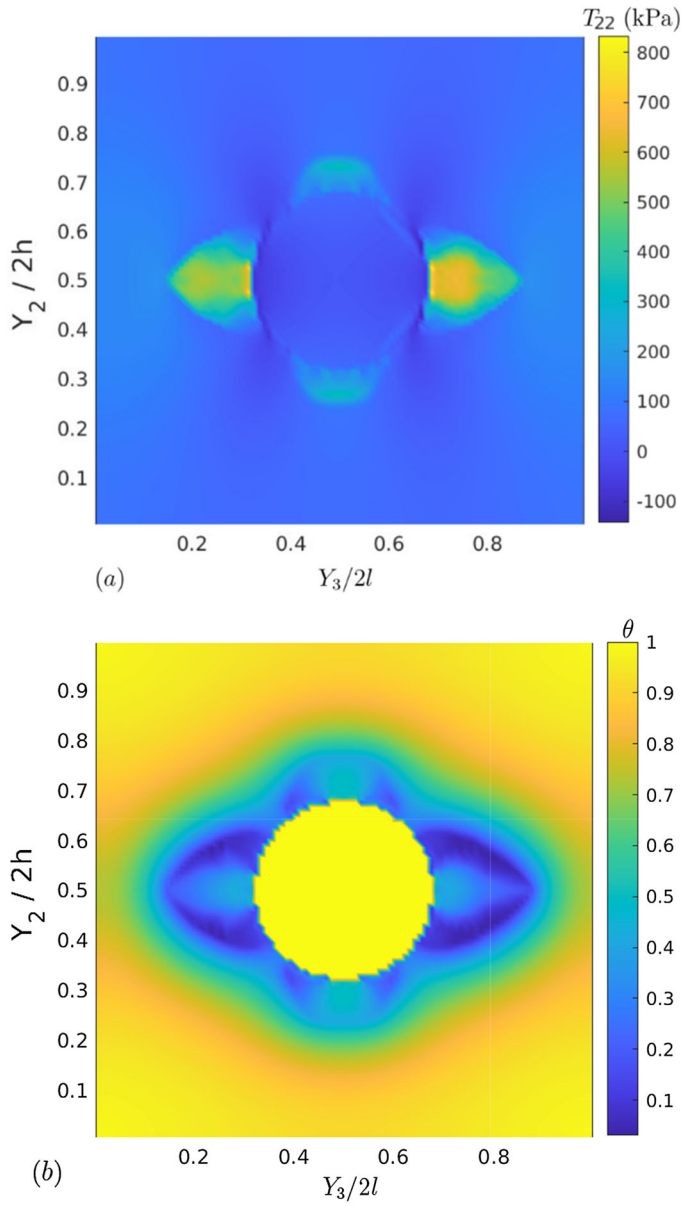

Fig. 11 A BK/modified Yeoh composite with a circular fiber of $v_f = 0.1$ fiber volume fraction. **a** Stress (T_{22}) distribution. **b** Intact mass fraction θ distribution

like in common phase-field approaches. However, here the phase-field resembling equations are derived mechanistically, rather than being introduced from functional considerations, as common in mathematical physics. Moreover, the material-sink approach differs from the phase-field approach in some theoretical aspects, as discussed, for example, in Elishakoff and Volokh [14], and Volokh [28]. The FSHFGMC is specifically suited for composites, in which equilibrium can be assumed to be reached in the phases earlier than between the phases. This normal assumption of the HFGMC is challenging when addressing two-time-scales physics, as the one typical for damage mechanics, where rupture bonds occur faster than continuum deformation. To overcome the associated stiffness of the corresponding differential equations (manifested in singularity of the algebraic equations produced by the HFGMC discretization), a predictor–corrector scheme was employed. In addition for being more natural for composites, the HFGMC offers the advantage of providing the homogenized response.

Results were generated for various examples of porous continua and composites, and characteristic stress and damage profiles and maps were produced. A natural generalization of the approach would be to allow

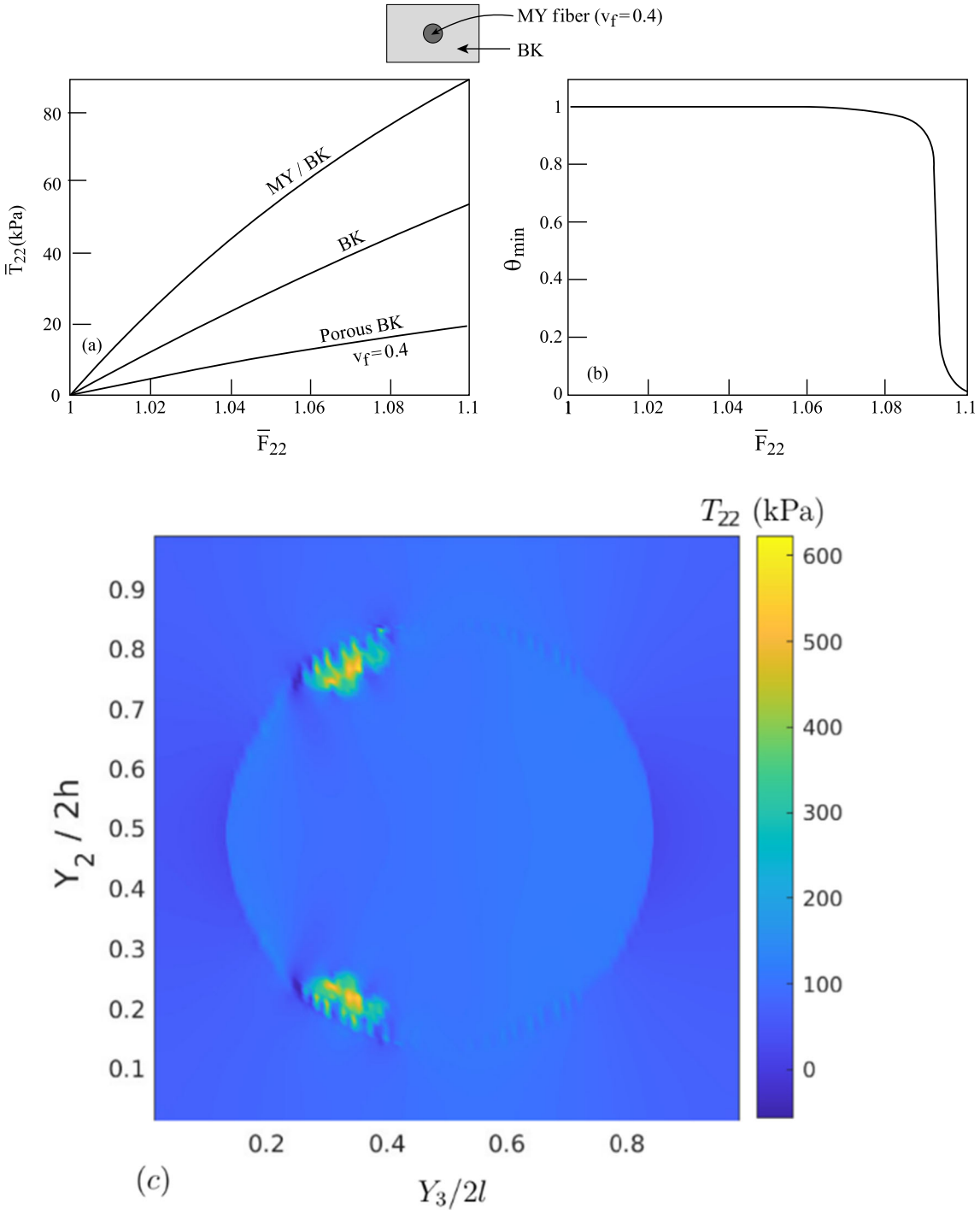

Fig. 12 A composite comprised of a BK matrix and a circular modified Yeoh fiber of $v_f = 0.4$ fiber volume fraction. **a** Global response $\bar{T}_{22} - \bar{F}_{22}$ of the composite, the behavior of the unreinforced BK material and the effective response of a porous BK material. **b** Plot of $\theta_{\min}$ against $\bar{F}_{22}$. **c** Stress (T_{22}) distribution

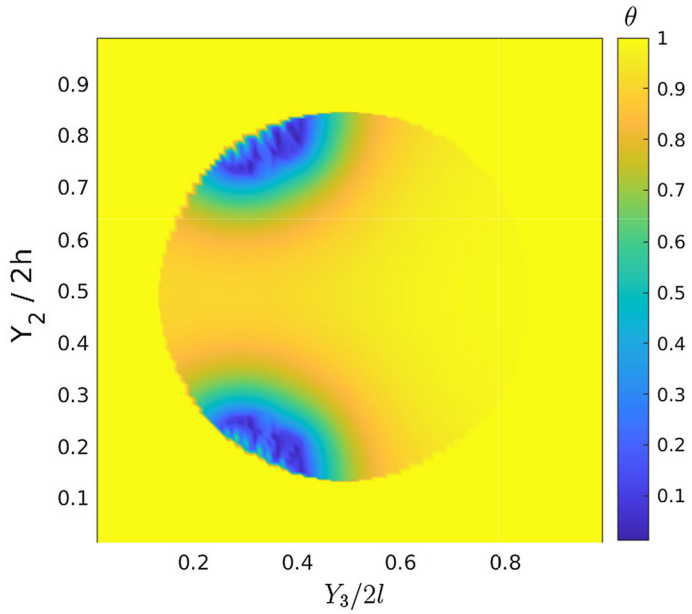

Fig. 13 Intact mass fraction θ distribution

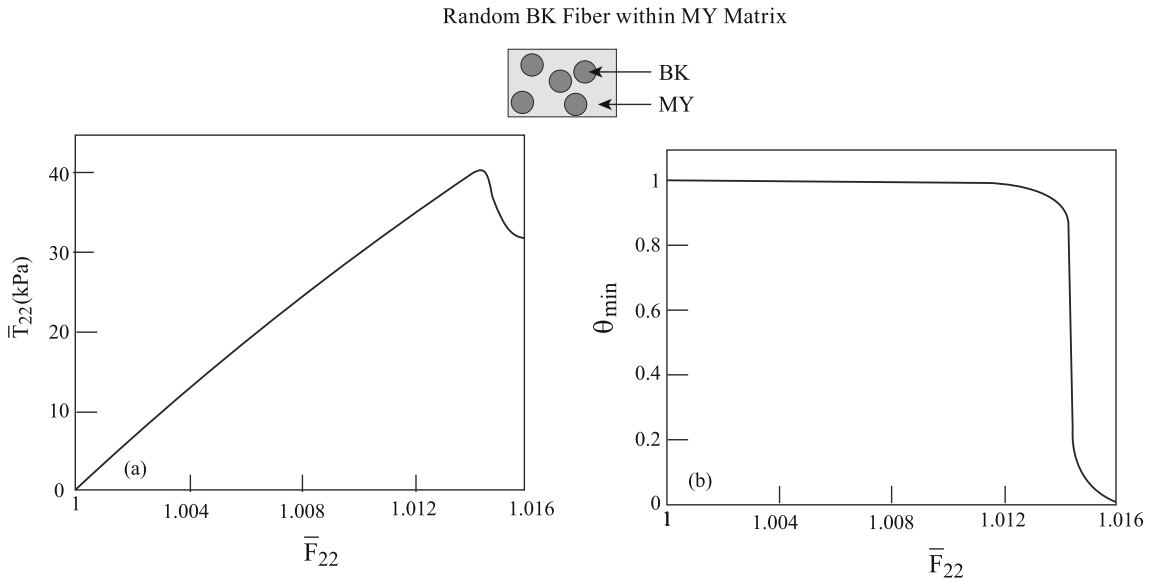

Fig. 14 A BK/modified Yeoh composite with several random circular BK fibers with an overall volume ratio of $v_f = 0.4$. **a** Global response $\bar{T}_{22} - \bar{F}_{22}$. **b** Plot of $\theta_{\min}$ against $\bar{F}_{22}$

non-uniform material characteristics in the periodic composite, leading to localization of damage on the RUC level, breaking the periodicity, similarly to what was done in [21]. Another generalization would be to account for thermal and dynamic effects, which is planned for future work.

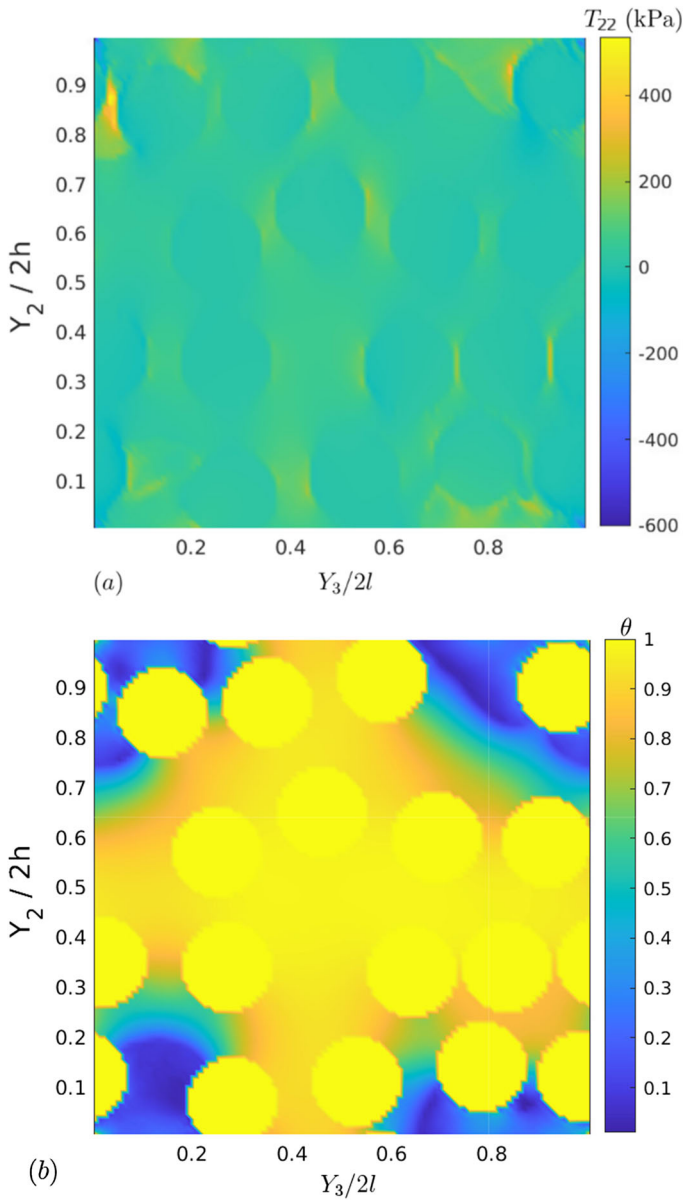

Fig. 15 A BK/modified Yeoh composite with several random circular BK fibers with an overall volume ratio of $v_f = 0.4$. **a** Stress (T_{22}) distribution. **b** Intact mass fraction θ distribution

Acknowledgements KYV gratefully acknowledges the support from the Israel Science Foundation (ISF-394/20).

Declarations

Conflict of interest The authors have no competing interests to declare.

References

1. Aboudi, J.: Finite strain micromechanical analysis of rubber-like matrix composites incorporating the Mullins damage effect. Int. J. Damage Mech **18**, 5–29 (2009)
2. Aboudi, J., Arnold, S.M., Bednarcyk, B.A.: Micromechanics of Composite Materials: A Generalized Multiscale Analysis Approach. Elsevier, Oxford (2013)
3. Aboudi, J., Volokh, K.Y.: Failure prediction of unidirectional composites undergoing large deformations. J. Appl. Mech. **82**, 071004-1–15 (2015)

4. Aboudi, J., Volokh, K.Y.: Modeling deformation and failure of viscoelastic composites at finite strains. Mech. Soft Mater. **2–12**, 2020 (2020)
5. Abu-Qbeitah, S., Jabareen, M., Volokh, K.Y.: Dynamic versus quasi-static analysis of crack propagation in soft materials. ASME. J. Appl. Mech. **89**(12), 121008 (2022)
6. Abu-Qbeitah, S., Jabareen, M., Volokh, K.Y.: Quasi-static crack propagation in soft materials using the material-sink theory. Int. J. Mech. Sci. **248**, 108160 (2023)
7. Blatz, P.J., Ko, W.L.: Application of finite elastic theory to the deformation of rubbery materials. Trans. Soc. Rheol. **6**, 223–251 (1962)
8. Borden, M.J., Verhoosel, C.V., Scott, M.A., Hughes, T.J.R., Landis, C.M.: A phase-field description of dynamic brittle fracture. Comput. Methods Appl. Mech. Eng. **217–220**, 77–95 (2012)
9. Breiman, U., Meshi, I., Aboudi, J., Haj-Ali, R.: Finite strain parametric HFGMC micromechanics pf soft tissues. Biomech. Model. Mechanobiol. **19**, 2443–2453 (2020)
10. Breiman, U., Meshi, I., Aboudi, J., Haj-Ali, R.: Finite strain PHFGMC micromechanics with damage and failure. Acta Mech. **233**, 2615–2651 (2022)
11. Bui, T.Q., Hu, X.: A review of phase-field models, fundamentals and their applications to composite laminates. Eng. Fract. Mech. **248**, 107705 (2021)
12. Dean, A., Asur Vijaya Kumar, P.K., Reinoso, J., Gerendt, C., Paggi, M., Mahdi, E., Rolfes, R.: A multi phase-field fracture model for long fiber reinforced composites based on the Puck theory of failure. Compos. Struct. **251**, 112446 (2020)
13. Denli, F.A., Gültekin, O., Holzapfel, G.A., Dal, H.: A phase-field model for fracture of unidirectional fiber-reinforced polymer matrix composites. Comput. Mech. **65**, 1149–1166 (2020)
14. Elishakoff, I., Volokh, K.Y.: Centenary of two pioneering theories in mechanics. Math. Mech. Solids **26**, 1896–1904 (2021)
15. Faye, A., Lev, Y., Volokh, K.Y.: The effect of local inertia around the crack tip in dynamic fracture of soft materials. Mech. Soft Mater. **1**(4), 1–21 (2019)
16. Guillén-Hernández, T., García, I.G., Reinoso, J., et al.: A micromechanical analysis of inter-fiber failure in long reinforced composites based on the phase field approach of fracture combined with the cohesive zone model. Int. J. Fract. **220**, 181–203 (2019)
17. Hofacker, M., Miehe, C.: Continuum phase field modeling of dynamic fracture: variational principles and staggered FE implementation. Int. J. Fract. **178**, 113–129 (2012)
18. Malvern, L.E.: Intoduction to the Mechanics of Continuous Medium. Prentice-Hall, Englewood-Cliff (1969)
19. Menikoff, R., Kober, E.: Equation of state and Hugoniot locus for porous materials: P-α model revisited. In: Furnish, M.D., Chhabildas, L.C., Hixson, R.S. (eds.) Shock Compression of Condensed Matter, pp. 129–132 (2000)
20. Mullins, L., Tobin, N.R.: Theoretical model for the elastic behavior of filled-reinforced vulcanized rubbers. Rubber Chem. Tech. **30**, 555–571 (1957)
21. Perchikov, N., Aboudi, J.: Micromechanical analysis of hyperelastic composites with localized damage using a new low-memory Broyden-step-based algorithm. Arch. Appl. Mech. **90**, 47–85 (2020)
22. Quinteros, M., García-Macíaz, E., Martínez-Pañeda, E.: Micromechanics-based phase field fracture modelling of CNT composites. Compos. Part B Eng. **236**, 109788 (2022)
23. Rao, S., Budzik, M.K., Dias, M.A.: On microscopic analysis of fracture in unidirectional composite material using phase field modelling. Compos. Sci. Technol. **220**, 109242 (2022)
24. Sangaletti, S., Garciá, I.G.: Fracture tailoring in 3D printed continuous fibre composite materials using the Phase field approach for fracture. Compos. Struct. **300**, 116127 (2022)
25. Tarafder, P., Dan, S., Ghosh, S.: Finite deformation cohesive zone phase field model for crack propagation in multi-phase microstructures. Comput. Mech. **66**, 723–743 (2020)
26. Volokh, K.Y.: Mechanics of Soft Materials. Springer (2016)
27. Volokh, K.Y.: Fracture as a material sink. Mater. Theory **1**(3), 1–9 (2017)
28. Volokh, K.Y.: New approaches to modeling failure and fracture of rubberlike materials. In: Fatigue Crack Growth in Rubber Materials. Advances in Polymer Science, vol. 286, pp. 131–152. Springer (2021)
29. Zhang, P., Hu, X., Yang, S., Yao, W.: Modelling progressive failure in multi-phase materials using a phase field method. Eng. Fract. Mech. **209**, 105–124 (2019)